IX Всероссийская Диановская конференция по волоконной оптике

Оптические запоминающие устройства в интегральном исполнении на основе фазопеременных материалов

к.т.н., нач. лаб.
Лазаренко П.И.

Пермь, 2023

National Research University of Electronic Technology

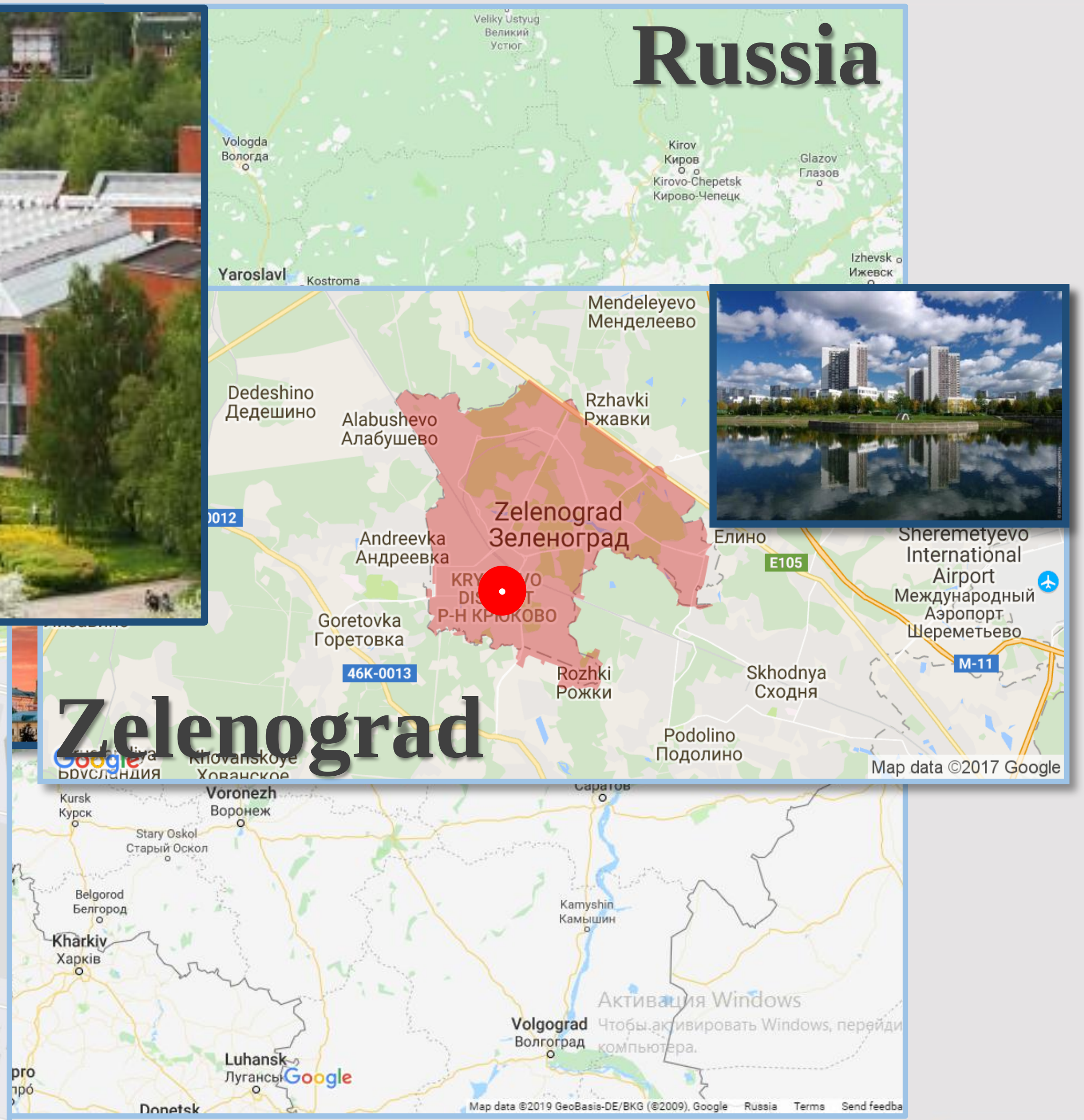

Development and Fabrication

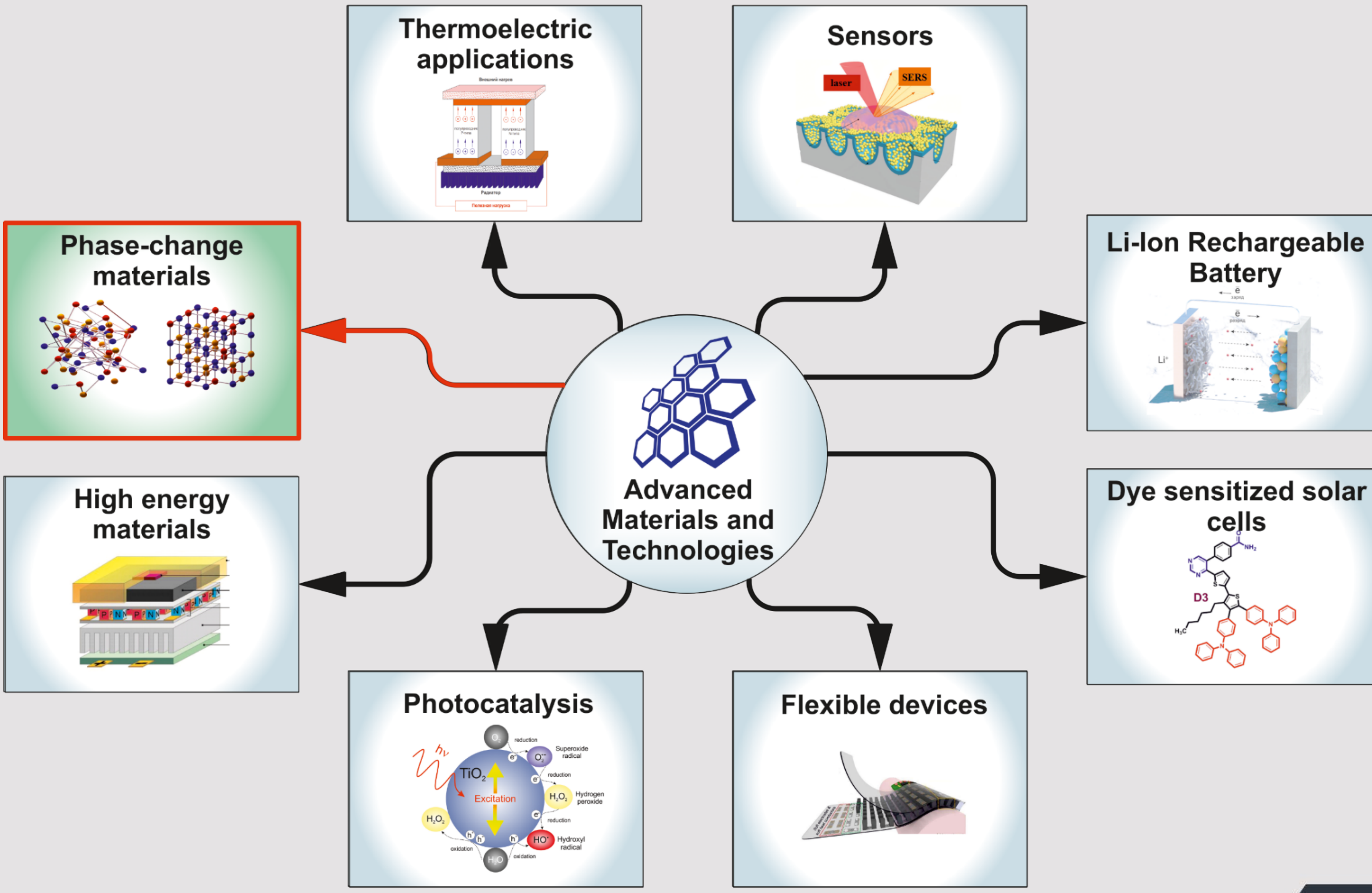

«Материалы и устройства активной фотоники»

Научно-исследовательская лаборатория

Направления научных исследований

Перестраиваемые элементы фотоники

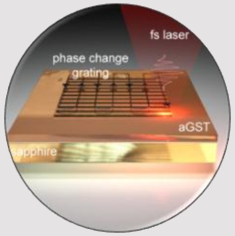

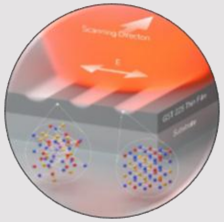

Инженерия поверхности, лазерная модификация

Интегральные фотонные элементы

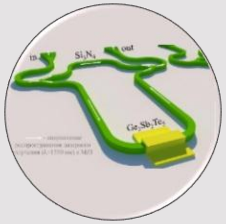

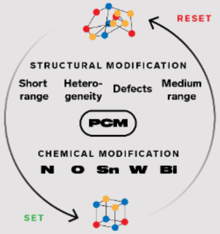

Материалы, фазовые превращения, моделирование

Laboratory Active Photonic Materials and Devices

Перестраиваемые энергонезависимые метаповерхности

Достоинства элементов:

- Реверсивное переключение;
- Энергонезависимость состояний;
- Малое энергопотребление (мДж/см^2);
- Материалы подходят для создания элементов, работающих на различных длинах волн, в том числе в видимом диапазоне спектра;
- Быстрое переключения (менее 100 нс);
- Многоуровневое управление сигналом за счет частичной кристаллизации.

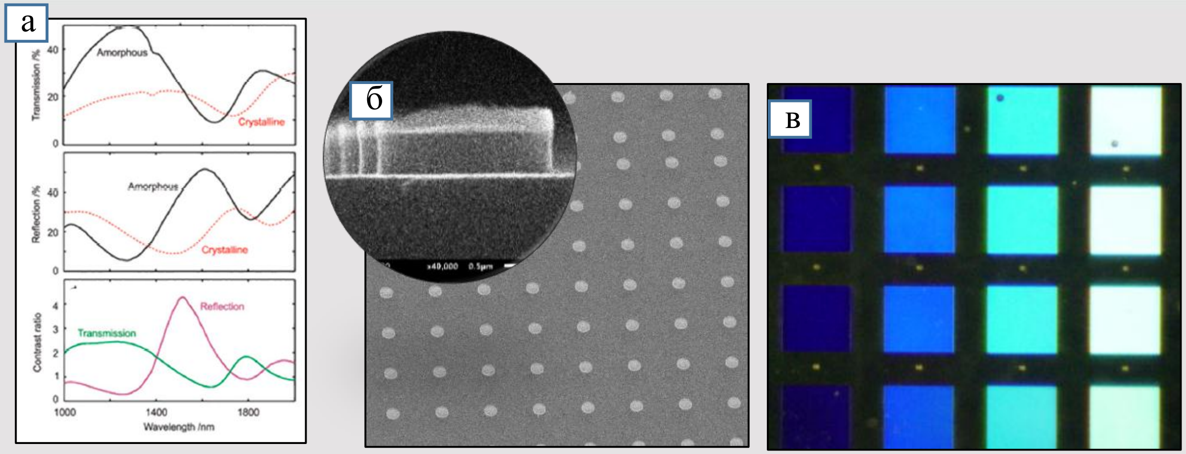

Рисунок 1 – Формируемые активные диэлектрические метаповерхности на основе изготавливаемых в НИУ МИЭТ халькогенидных тонкопленочных покрытий: (а) изменение оптических параметров структуры при изменении фазового состояния; (б) РЭМ изображение изготавливаемого элемента; (в) вид сформированных элементов в оптический микроскоп.

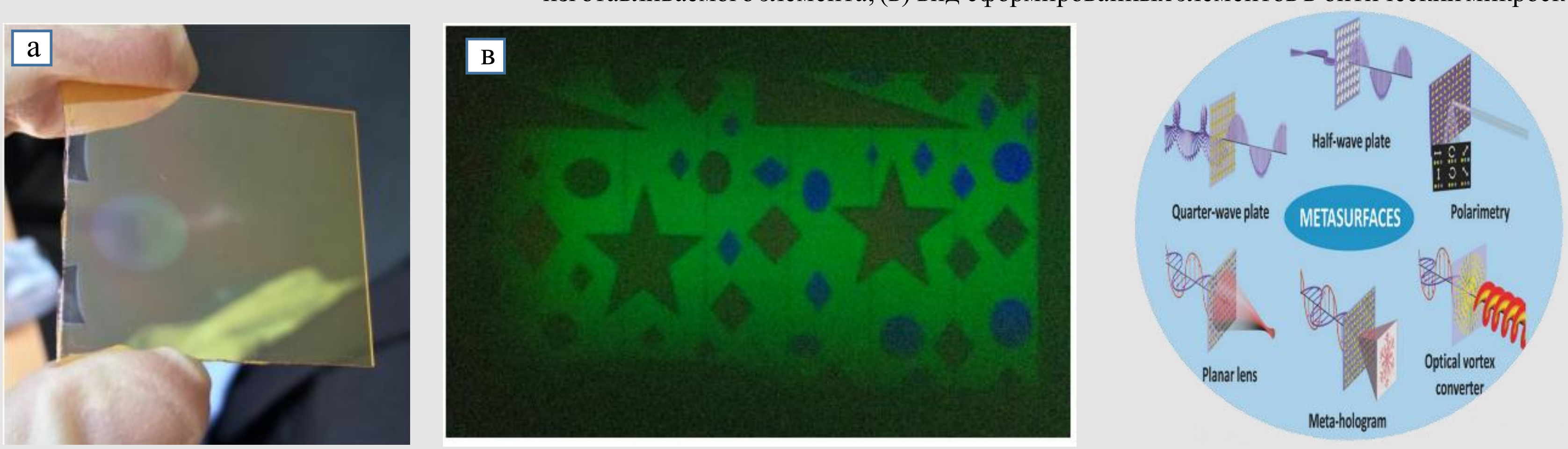

Рисунок 2 – На основе формируемых в НИУ МИЭТ халькогенидных тонкопленочных покрытий продемонстрирована возможность изготовления реконфигурируемых голографических элементов для систем дополненной реальности: (а) общий вид элемента; (б) спектр пропускания тонкой пленки; (в) демонстрация работа записанных голограмм.

[1] V. Borisov, et al. Chalcogenide thin films — holographic media for augmented reality devices // Applied Sciences (2022) in print.

Laser-induced Periodic Surface Structures

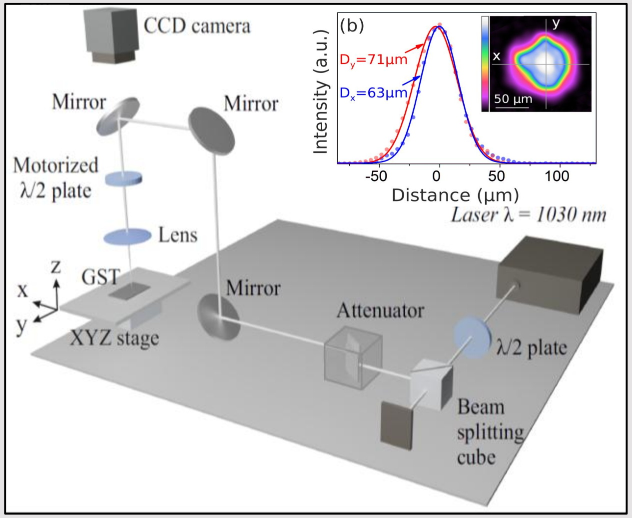

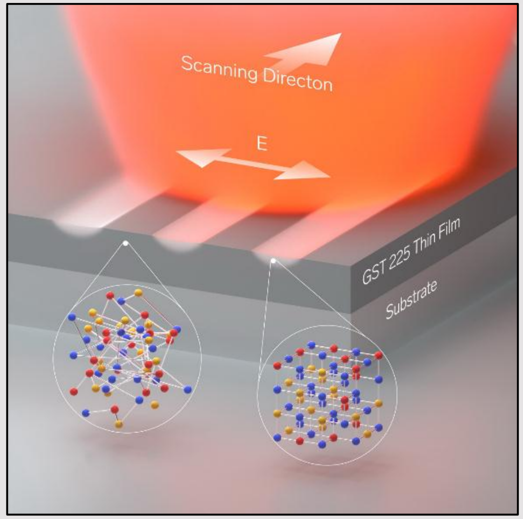

The scheme of the experimental setup and (b) formation of the binary grating on the GST surface by a scanning femtosecond beam

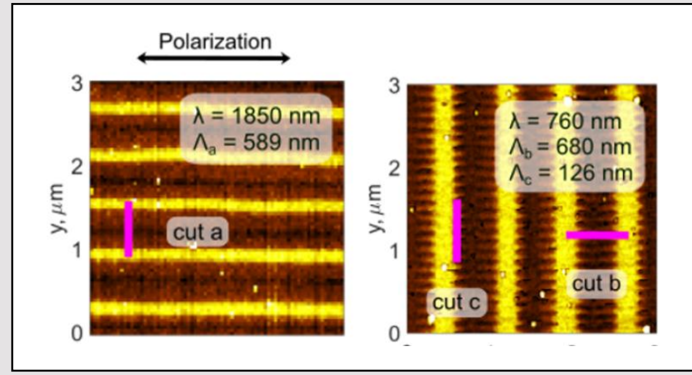

Result of the investigation using AFM

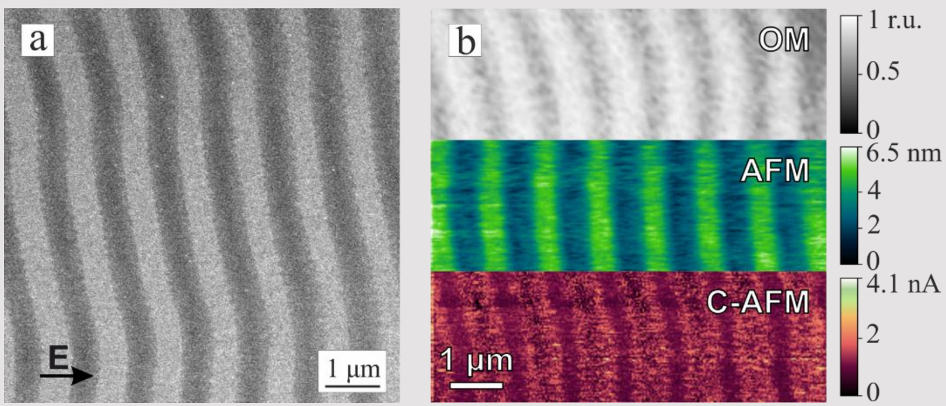

The results of the microscopy studies. E is the light field vector of the laser beam.

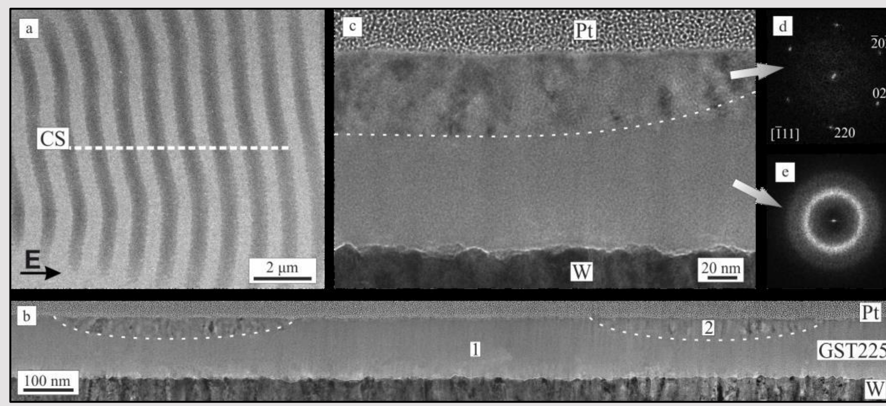

The results of the electron microscopy analysis: a) the SEM image; b,c) TEM images of the ripples profile at different scales.

[1] S. Kozyukhin, et al. Laser-induced modification and formation of periodic surface structures (ripples) of amorphous GST225 phase change materials // Optics and Laser Technology 113 (2019) 87–94

[2] S. Kozyukhin and et al. Specific Features of Formation of Laser-Induced Periodic Surface Structures on $Ge_2Sb_2Te_5$ Amorphous Thin Films under Illumination by Femtosecond Laser Pulses // PSS:B 257 (2020) P. 1900617

Two-Phase Binary Diffraction Gratings

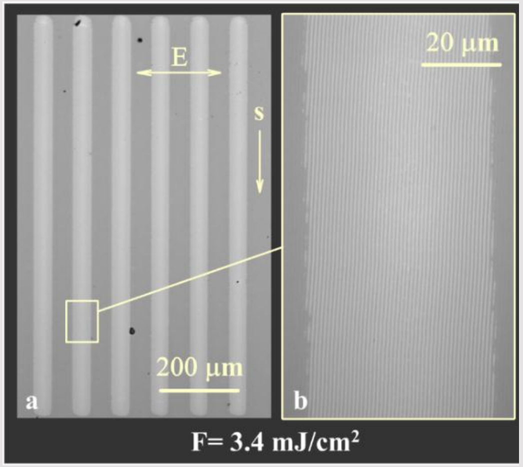

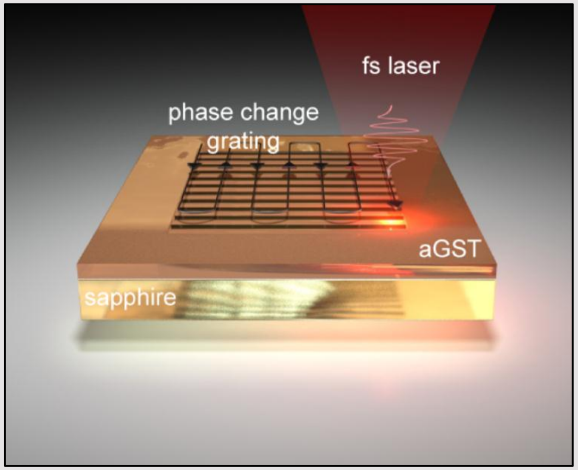

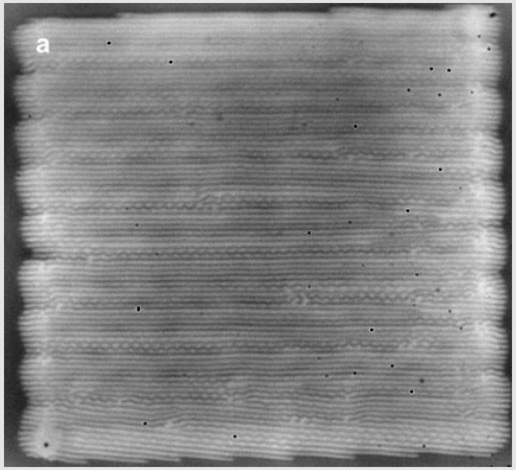

(a) The image of the stripes obtained by scanning with a fluence of $F = 3.4$ mJ/cm^2 at a speed $V_{sc} = 0.04$ mm/s.
(b) Zoomed structure of rippled Vector **s** indicates the direction of scanning, **E** shows the polarization of the light beam
(c) The scheme of the formation of the binary grating. (d) Large-scale quality of GST phase gratings.

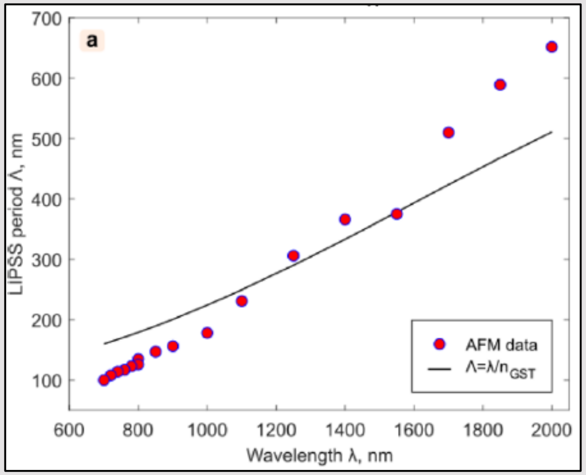

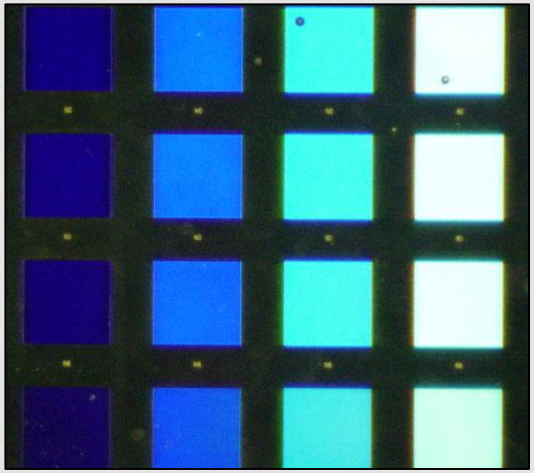

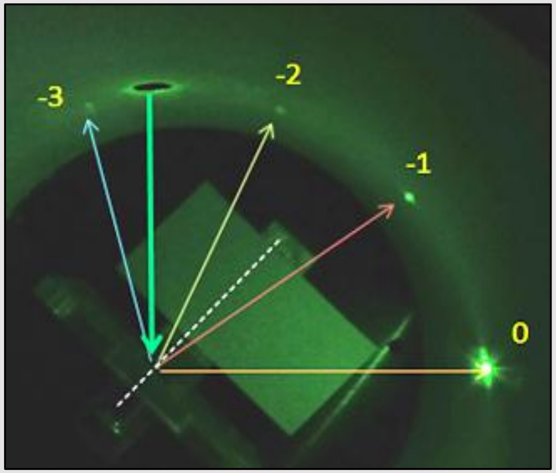

Fabricated Two-Phase Binary Diffraction Gratings

[1] P.I. Trofimov and et al. Rewritable and Tunable Laser-Induced Optical Gratings in Phase-Change Material Films // ACS Appl. Mater. Interfaces 13, 27 (2021) P. 32031–32036

[2] M. Smaev and et al. Direct Single-Pass Writing of Two-Phase Binary Diffraction Gratings in a $Ge_2Sb_2Te_5$ Thin Film by Femtosecond Laser Pulses// Apl. Surf. Sci. (2021) (submitted)

Фотонные интегральные элементы и схемы

Достоинства элементов:

- Реверсивное переключение;
- Энергонезависимость состояний;
- Малое энергопотребление (мДж/см^2);
- Рабочая длина волны 1550 нм;
- Длительность переключения менее 100 нс;
- Количество бит в ячейке более 3 бит;
- Возможность интегрального исполнения;
- Помехоустойчивость;
- Рабочий диапазон от -50 до 100 С;
- Совместимость с процессами кремниевой микроэлектроники.

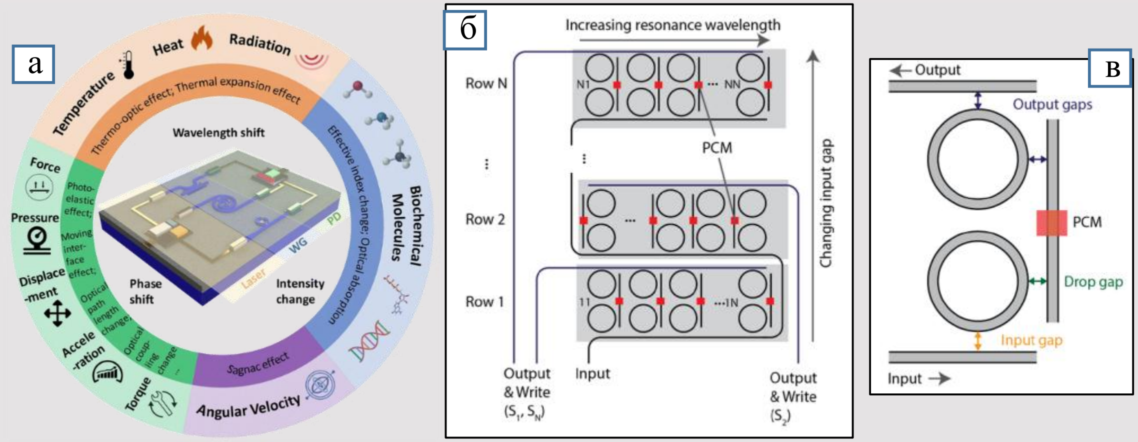

Рисунок 1 – Перспективы использования изготавливаемых элементов интегральной фотоники (а), а также схематичное изображение одного из прорабатываемых варианта планируемой к изготовлению логической фотонной интегральной схемы для полностью оптических нейроморфных вычислений

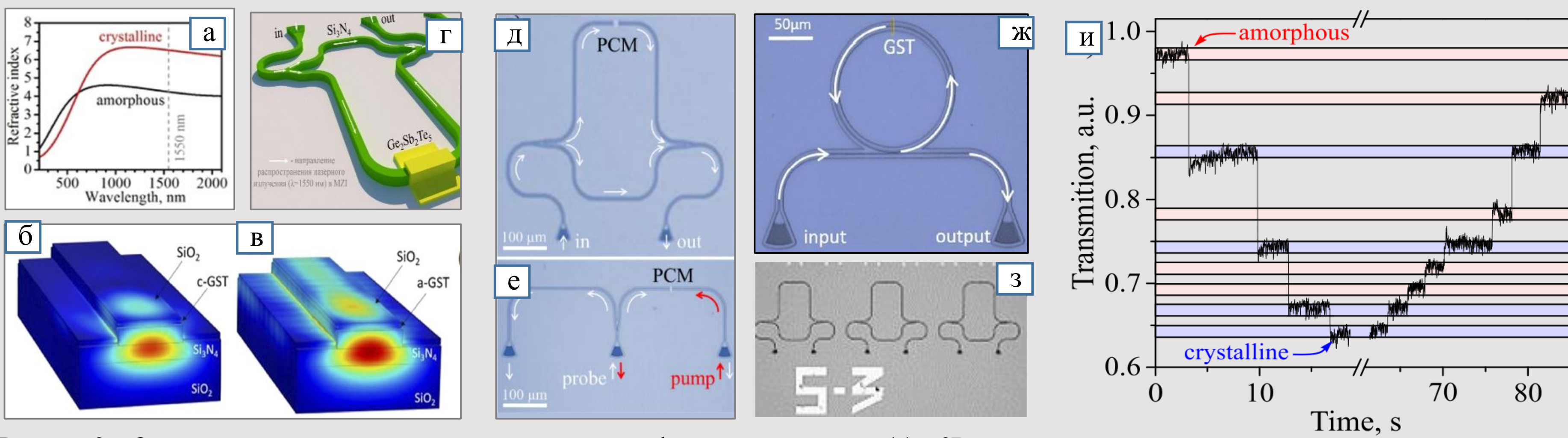

Рисунок 2 – Оптические параметры тонких пленок с разным фазовым состоянием (а) и 3D моделирование распределение интенсивности излучения в элементах на их основе (б-г). Изготовленные коллективом единичные элементы различного назначения, а также демонстрация возможности их реверсивного пеерключения между 9 различными логическими состояниями.

[1] P. Lazarenko, et al. Size effect of the $Ge_2Sb_2Te_5$ cell atop the silicon nitride O-ring resonator on the attenuation coefficient // APL Materials, vol. 9 (2021)

Интегральные фотонные элементы на основе фазопеременных материалов

Шерченков А.А.
в.н.с. НИУ МИЭТ

Козюхин С.А.
г.н.с. ИОНХ РАН
зав.каф. МФТИ

Светухин В.В.
чл.-корр. РАН
дир. НПК «ТЦ»

Колобов А.В.
дир.инст. РГПУ

Гольцман Г.Н.
зав. каф. МПГУ
зав. каф. ВШЭ

Dr. V. Takáts
ATOMKI

Ковалюк В.В.
с.н.с. МПГУ
нач.лаб. МИСИС

Якубов А.О
м.н.с.
НИУ МИЭТ

Кицюк Е.П.
нач.лаб.
НПК «ТЦ»

Смаев М.П.
с.н.с.
ФИАН РАН

Глухенькая В.Б.
м.н.с.
МИЭТ

Федянина М.Е.
м.н.с.
МИЭТ

Phase change memory

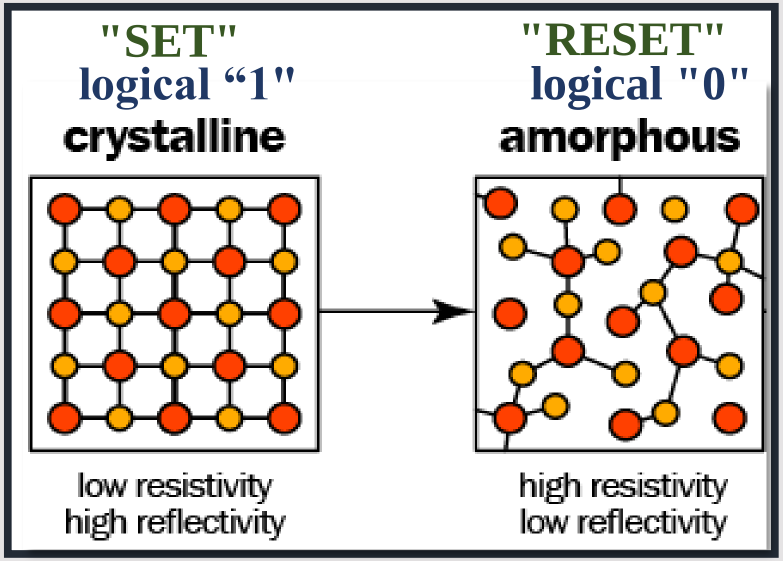

The chalcogenide $Ge_2Sb_2Te_5$ (GST225) is one of several functional materials which has already been in wide use for different purposes, in particular, for optical discs (DVD, Blu-Ray) and electrical memory (PRAM). Also it is one of the best materials for non-volatile memory and neuro-inspired computing chips.

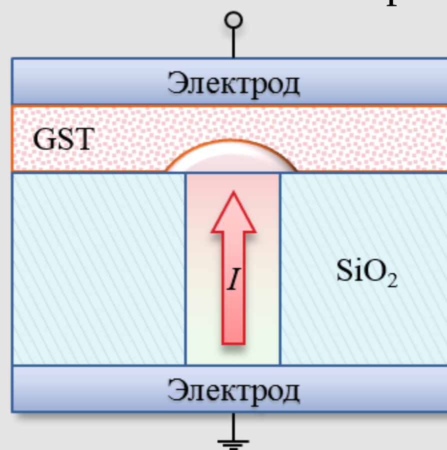

PCM cell structure

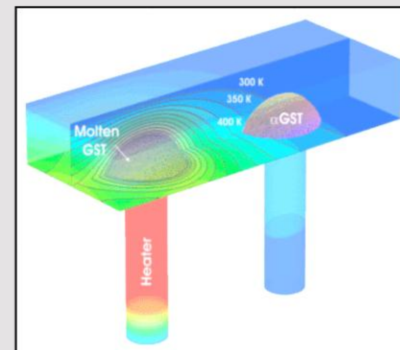

Temperature 3D-model for writing operation of logical "0"

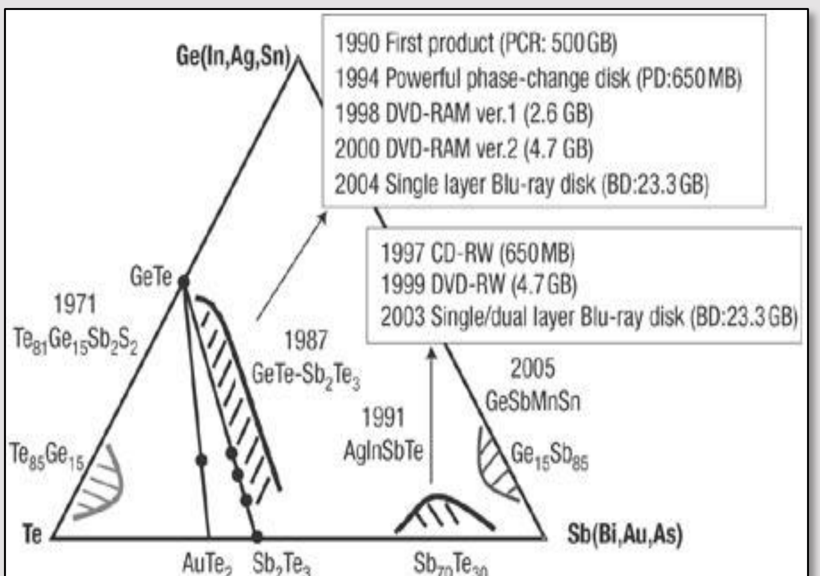

Phase diagram of Ge-Sb-Te system

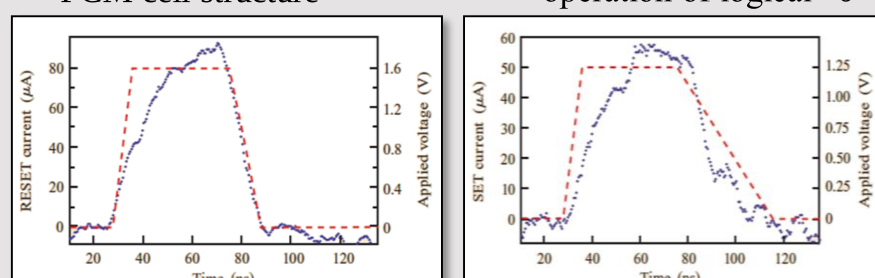

The writing and erasing operations in PCM devices

Electrical properties

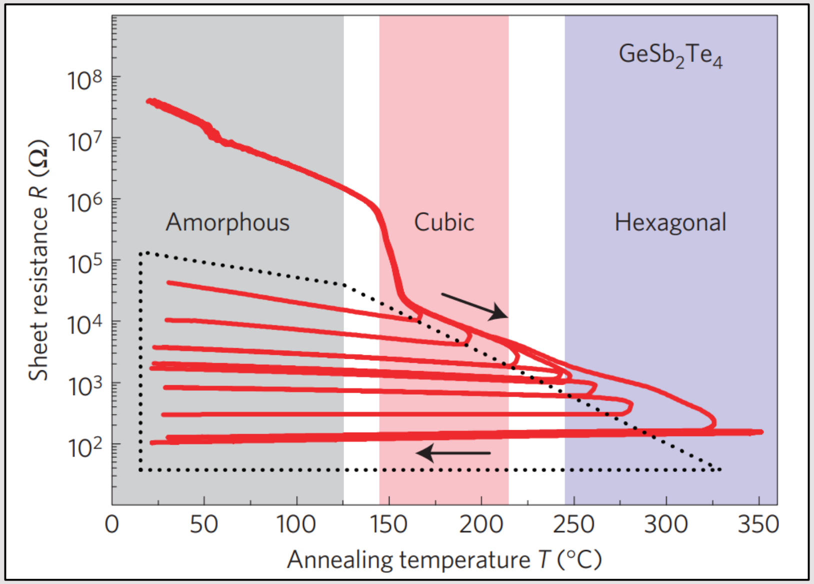

The advantages of Ge-Sb-Te (GST) materials:

1. Rapid phase transitions (< 50 ns).
2. Sufficient stability of phase state (> 10 years).
3. Significant change of the properties ($>10^3$ Ohm·cm).
4. High radiation resistance .
5. Small cell size ($4F^2$).

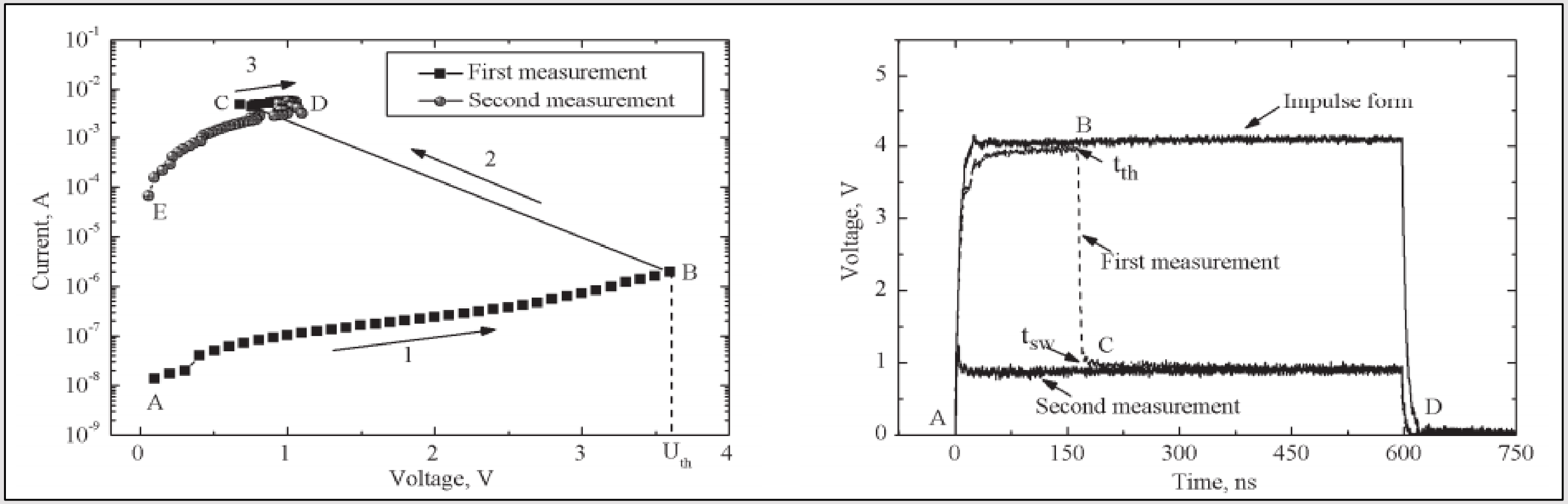

Results of DC and impulse measurements for GST225 thin films.

[1] P. Lazarenko Electrical properties of the $Ge_2Sb_2Te_5$ thin films for phase change memory application // AIP Conference Proceedings, 172721 (2016) P. 020013

How does it work?

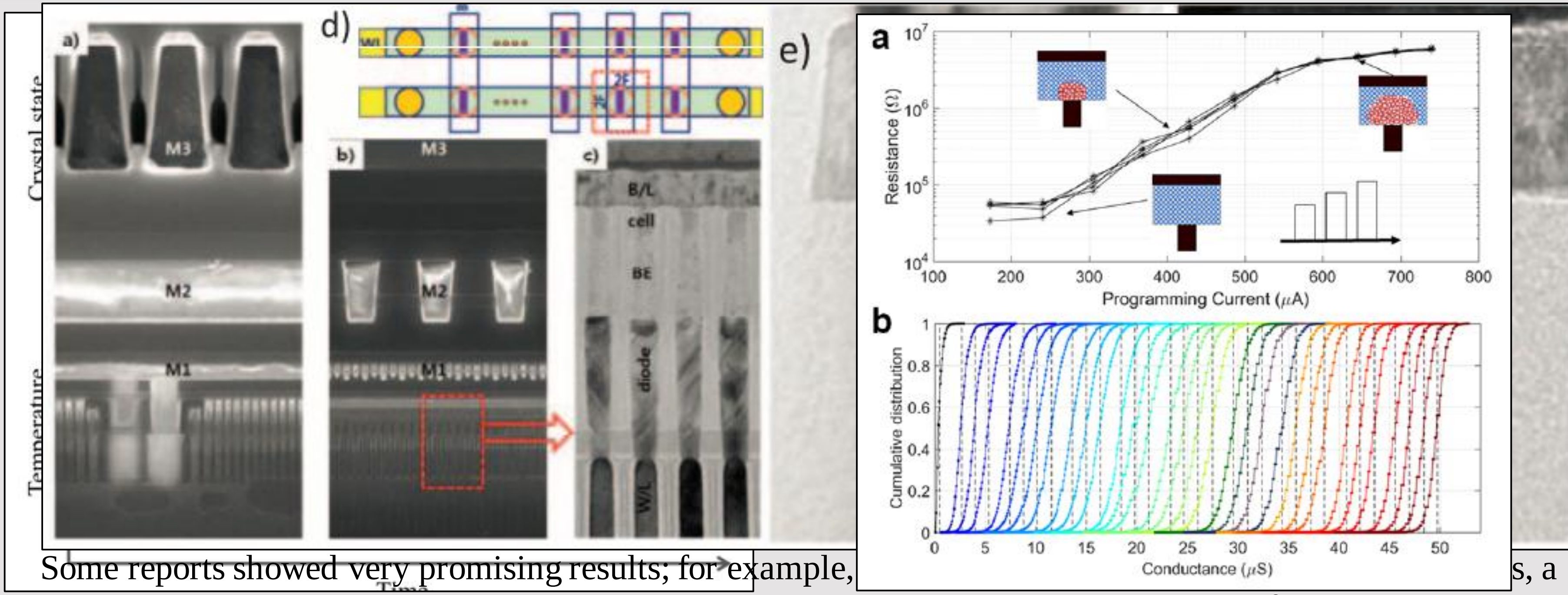

Some reports showed very promising results; for example, … s, a write latency of 150 ns, and a write cyclic endurance of more than 10^9.

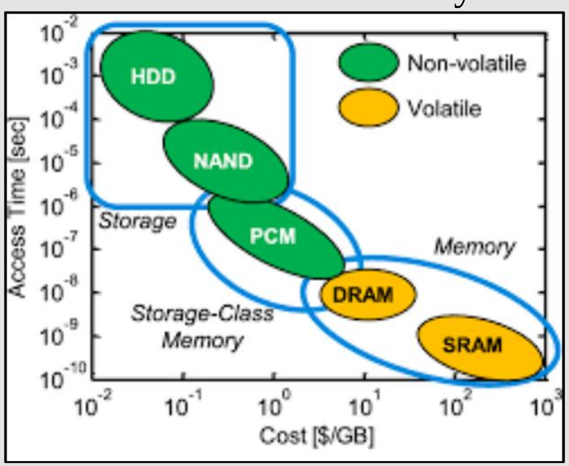

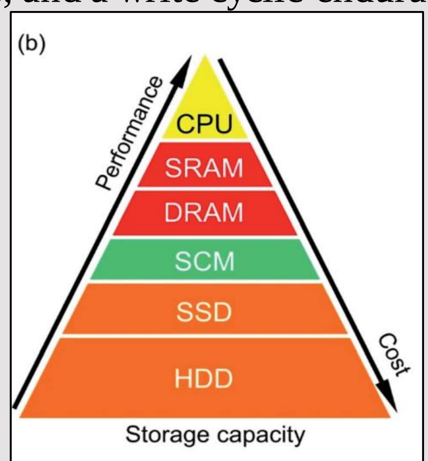

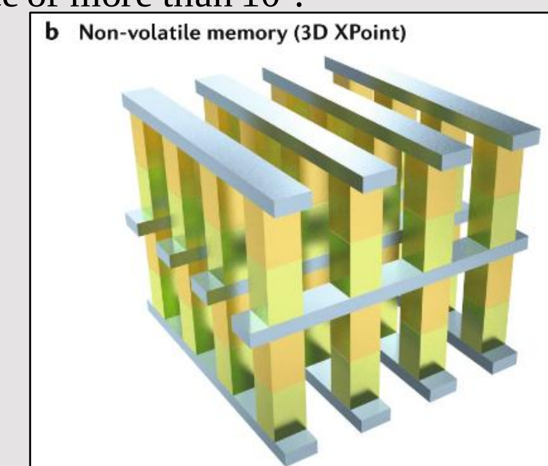

[1] G.W. Burr, et al. Recent Progress in Phase-Change Memory Technology, IEEE 6(2), (2016) P. 146-162.

Flexible PCM devices

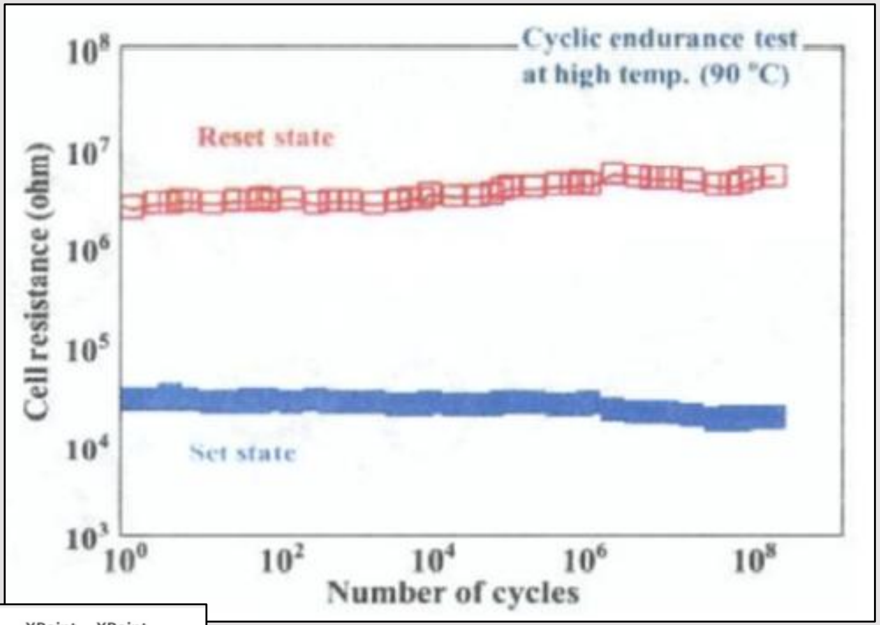

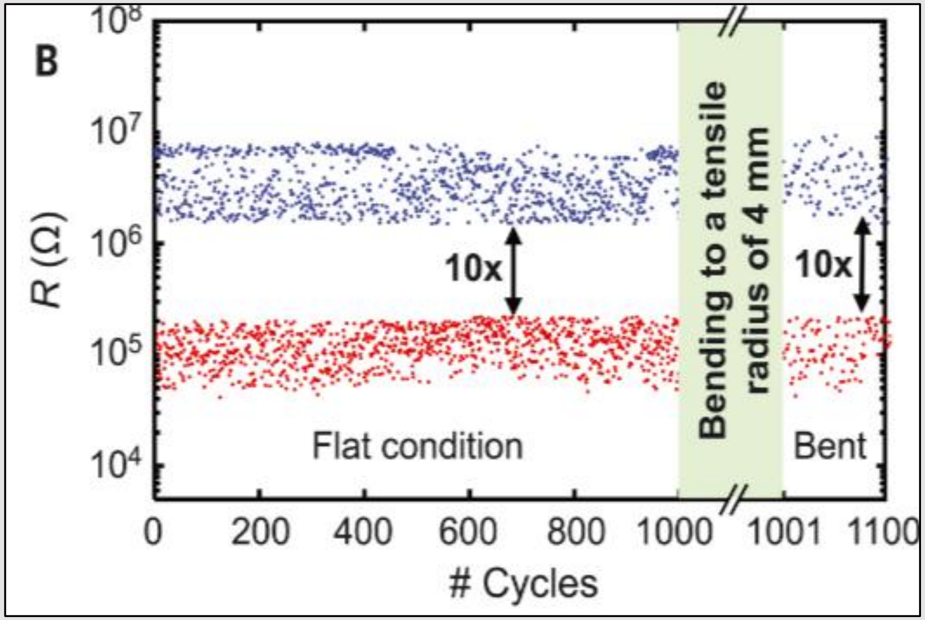

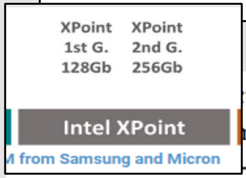

…teristics of non-volatile memory (NVM) technologies in comparison with dynamic …emory (DRAM) and NAND flash memory.

	DRAM	STT-MRAM	PCM	NAND Flash
Maturity	Product	Prototype	Product	Product
Read latency	10 ns	10 ns	20–50 ns	25 us
Write latency	10 ns	10 ns	80–500 ns	200 us
Erase latency	N/A	N/A	N/A	200 ms
Energy per bit access (r/w)	2 pJ	0.02 pJ	20pJ/100 pJ	10 nJ
Static power	Yes	No	No	No
Endurance (writes/bit)	10^{16}	10^{16}	10^6–10^8	10^5
Cell size	6–8 F^2	>6 F^2	5–10 F^2	4–5 F^2
MLC	N/A	4 bits/cell	4 bits/cell	4 bits/cell

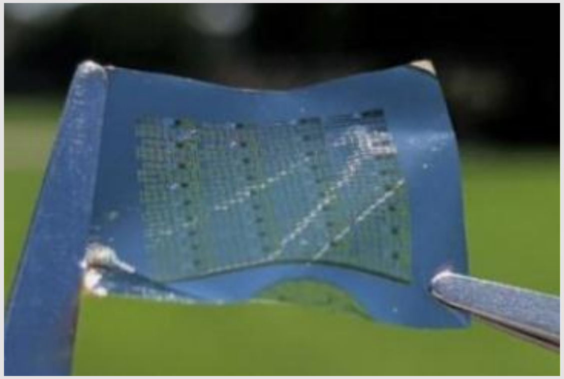

Cho H. Implications of NVM Based Storage on Memory Subsystem Management (2020) / 10.3390/app10030999

Non-volatile optical devices

Block diagram of the optical system

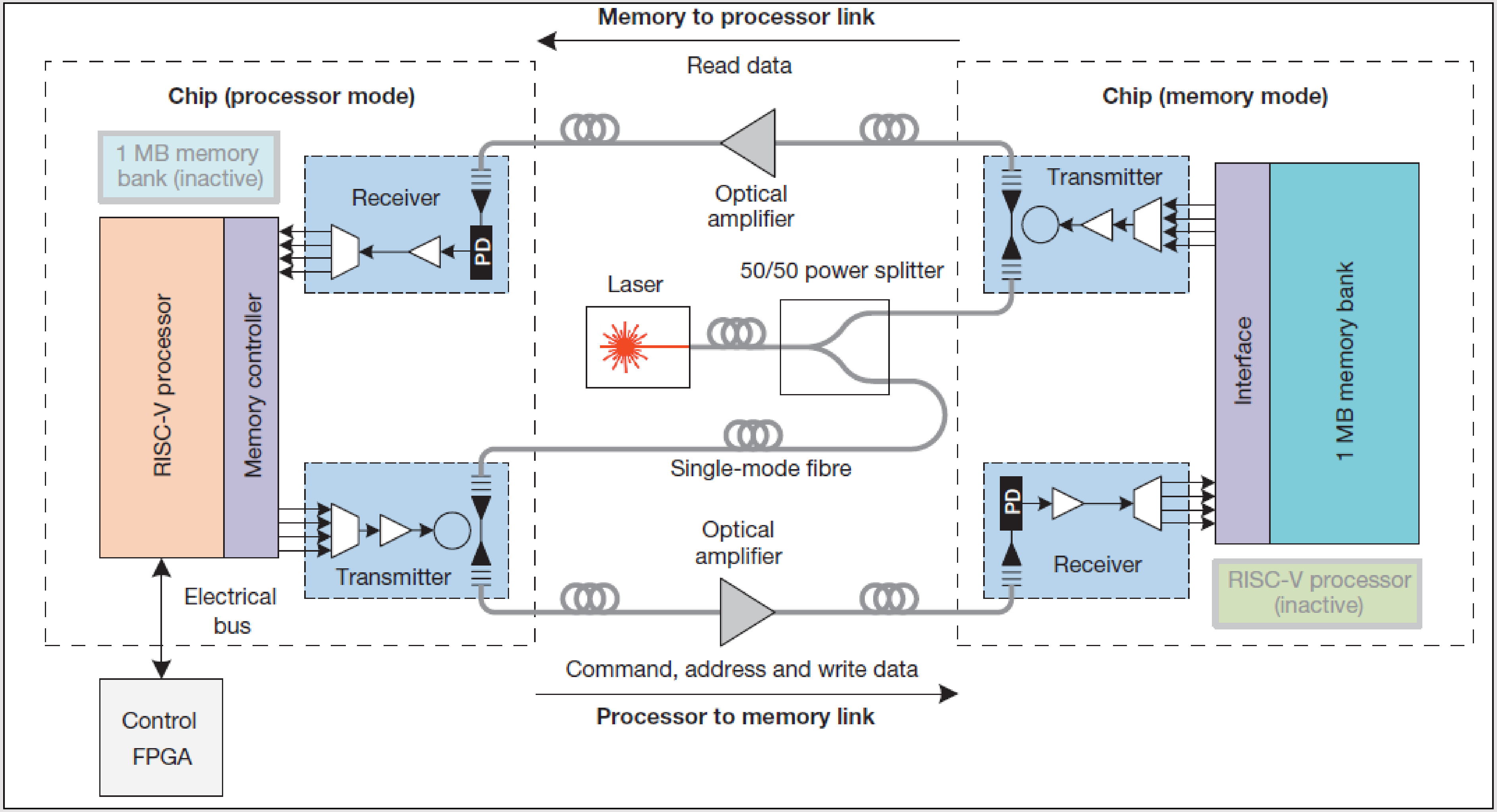

The system uses one chip acting as the processor and the other acting as memory, connected by a full-duplex optical link with a round-trip distance of 20 m by fibre.

[1] Sun, C. et al. Single-chip microprocessor that communicates directly using light // Nature, 528 (2015) 534–538

Nonvolatile transmission modulation

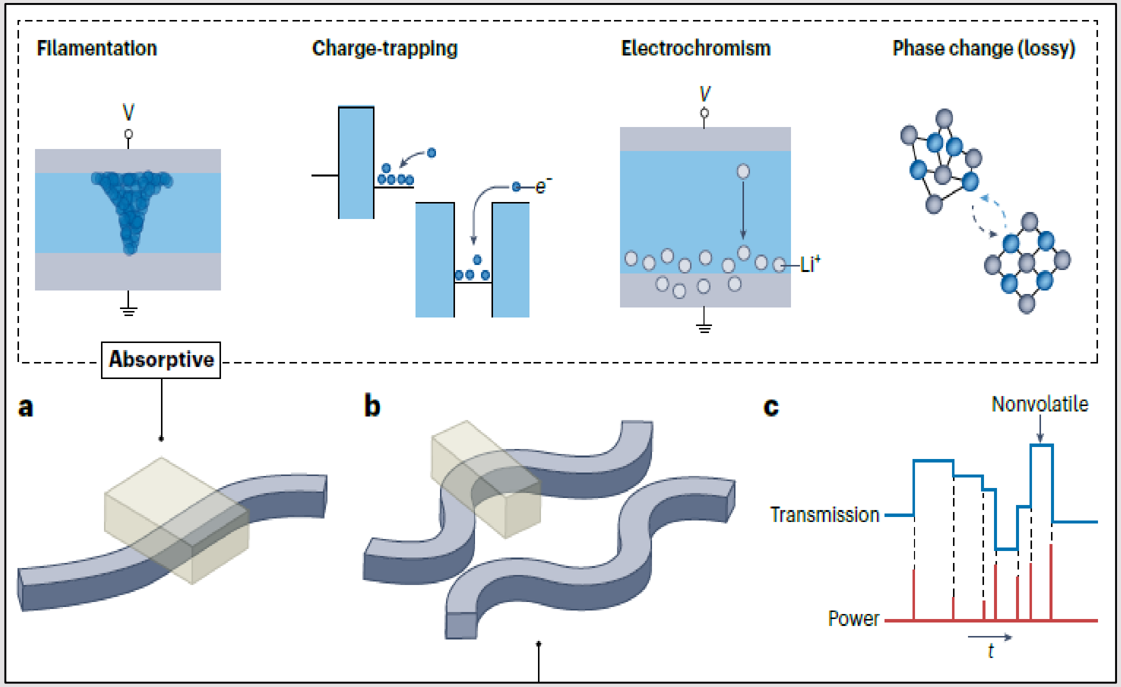

Technological features:

- Lattice coherency;
- Adhesion strength;
- Electrical contact type;
- Temperature processing compatibility,
- Avoiding interfacial defects;
- CMOS compatibility.

The performance parameters:

- Retention time and stability;
- Programming speed;
- Modulation depth;
- Cyclability;
- Footprint,
- Power consumption;
- Cost.

[1] N.Youngblood et al. Integrated optical memristors // Nature Photonics (2023)

Performance metrics

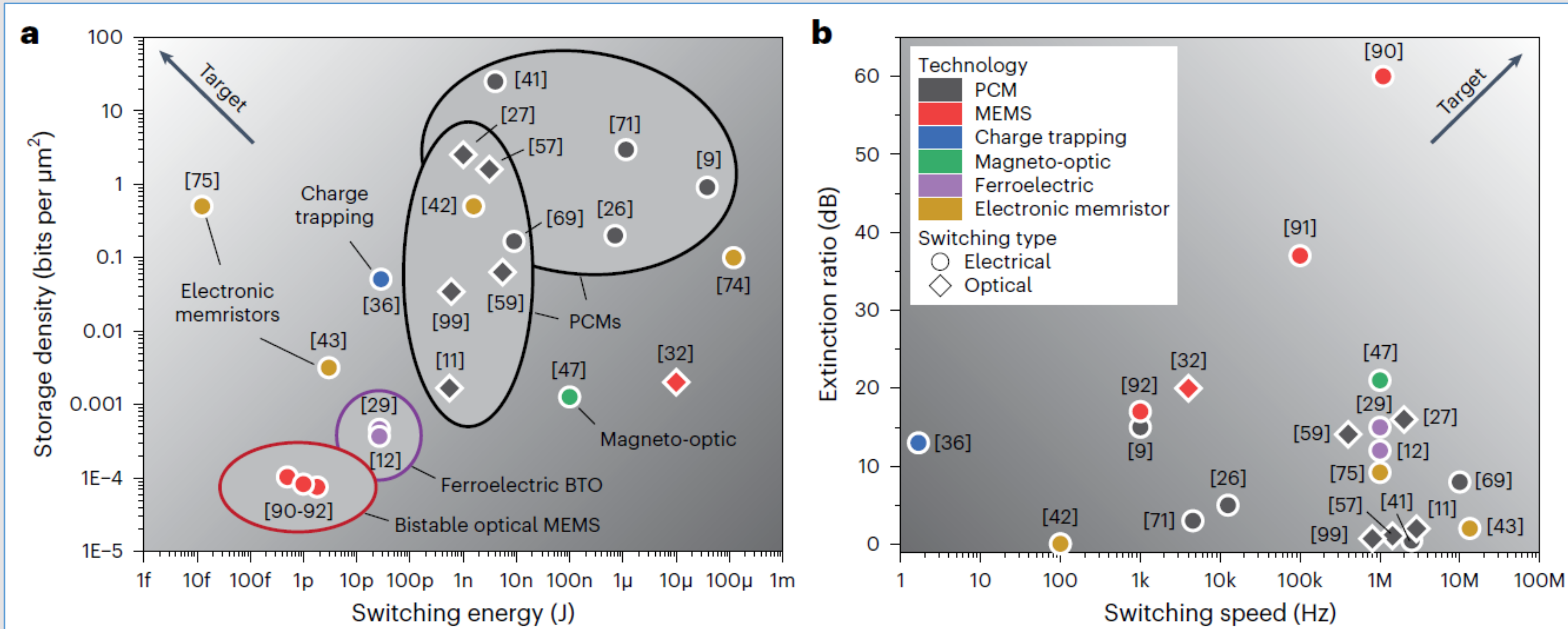

Technology (E/O switched)	Switching speed[a]	Switching energy[a]	Bits stored	Footprint (μm²)	ER[b] (dB)	Insertion loss (dB)	Max. cycles
MEMS (O)	4 kHz	10 μJ	1 bit	400	20	1	>30
MEMS (E)	0.1–1 MHz	0.5–1 pJ	1 bit	>10,000	60	>0.025	10^{10}
Memristor (E)	1 MHz	12.5 fJ	1 bit	2	9.2	25	>10^3
MO (E)	1 MHz	100 nJ	>3 bits	8,000	21	2.5	>7
Ferroelectric (E)	1 MHz	30 pJ	>3 bits	>20,000	12	>0.07	300
Trapped charge (E)	1 Hz	30 pJ	4 bits	315	13	2	>30
PCM (E)	1–10 MHz	4 nJ–10 μJ	4 bits	1–500	0.5–15	>0.4	5×10^5
PCM (O)	1–10 MHz	0.1–1 nJ	6 bits	1–310	0.7–16	>0.75	10^6

[1] N.Youngblood et al. Integrated optical memristors // Nature Photonics (2023)

Optical memory devices

ЭнергоНЕзависимые

Энергозависимые

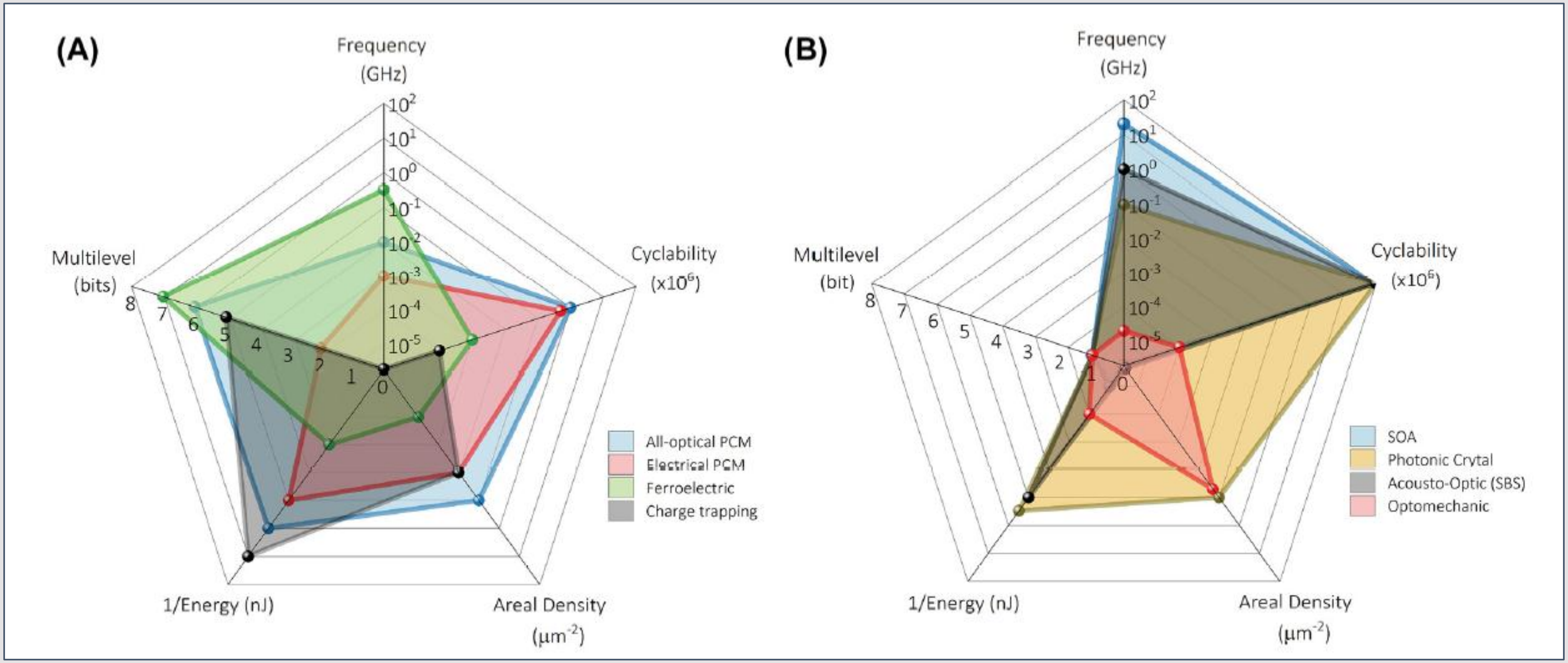

[1] C. Lian, et al. Photonic (computational) memories: tunable nanophotonics for data storage and computing // Nanophotonics 2022. - P. 3823–3854

Optical properties of GST225 thin films

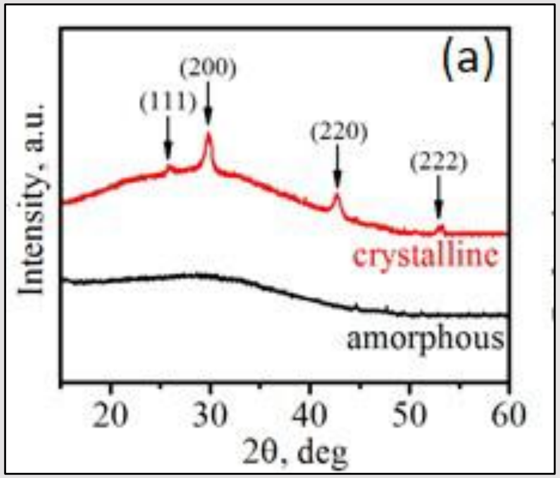

The XRD spectra of the as-deposited and annealed $Ge_2Sb_2Te_5$ films

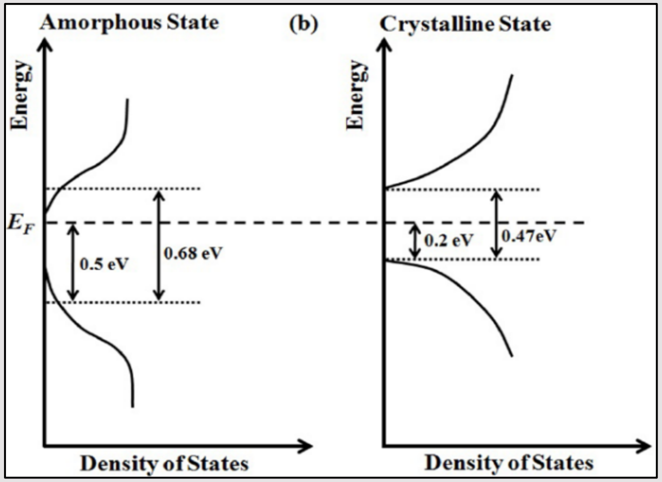

Simplified band gap diagrams for amorphous and crystalline GST films

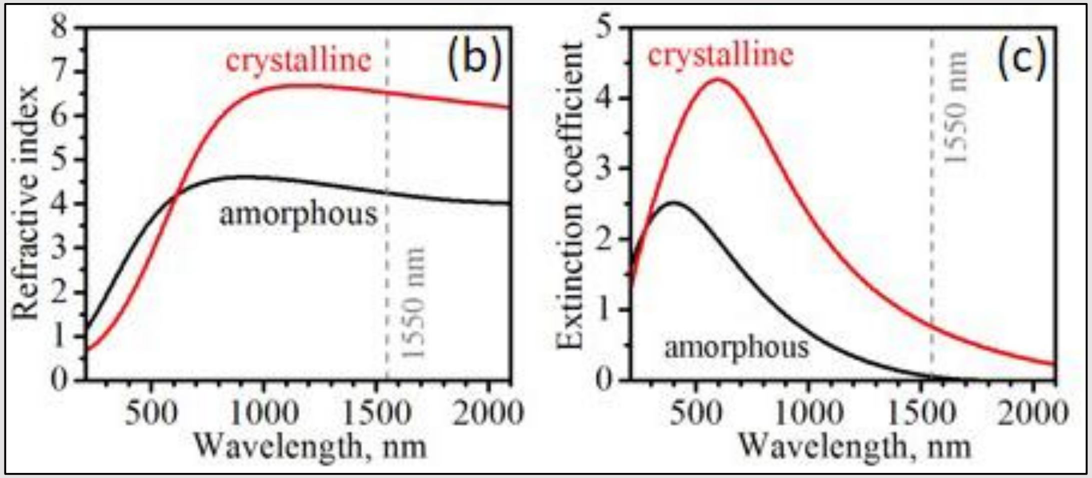

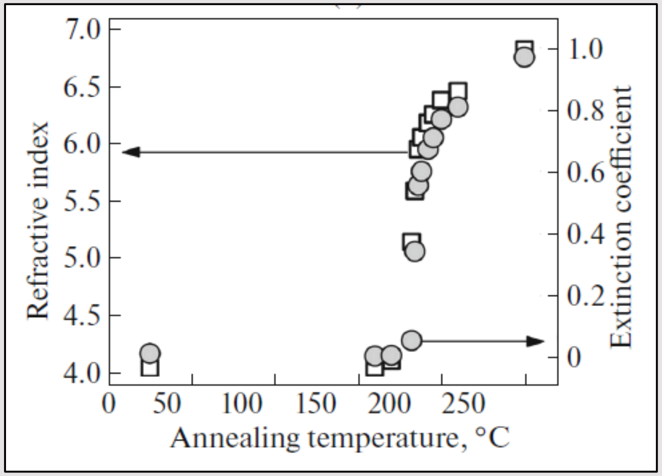

(b) The spectra of the refractive index for the amorphous and crystalline GST films; (c) The spectra of the extinction coefficient for the amorphous and crystalline GST films.

Optical properties of GST225 thin films

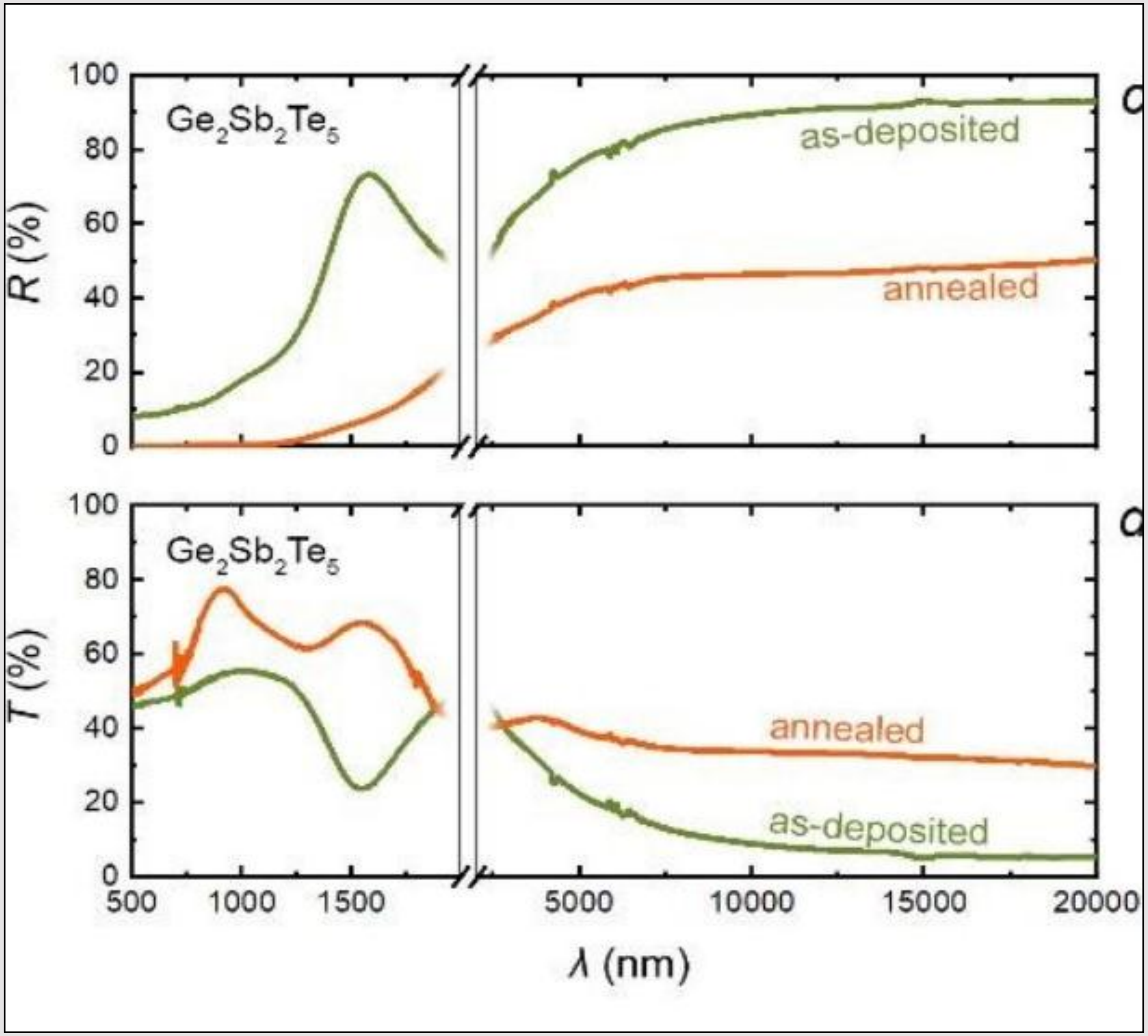

[1] A. V. Kiselev et al. Dynamics of reversible optical properties switching of $Ge_2Sb_2Te_5$ // Optics & Laser Technology (2022)

Phase change memory

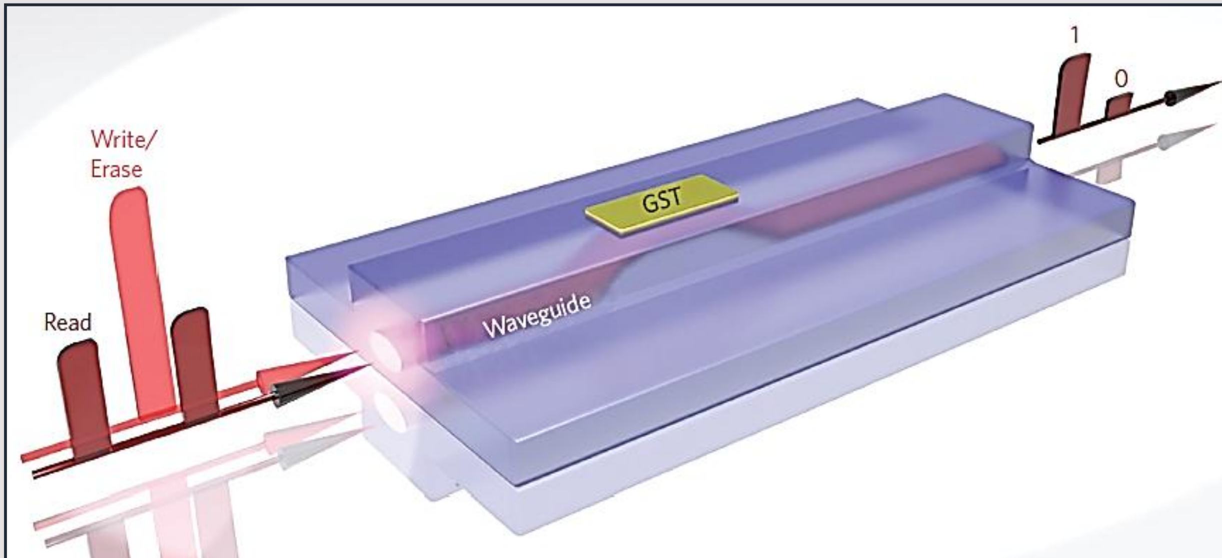

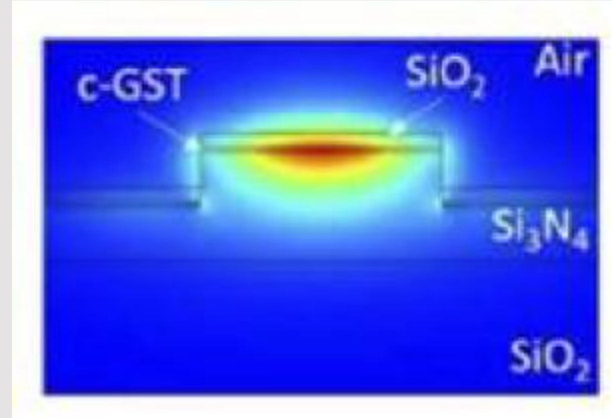

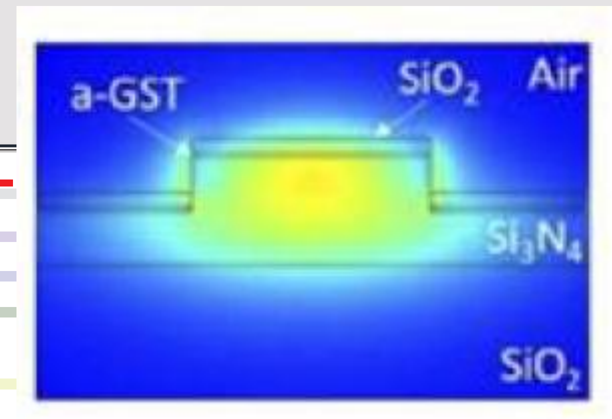

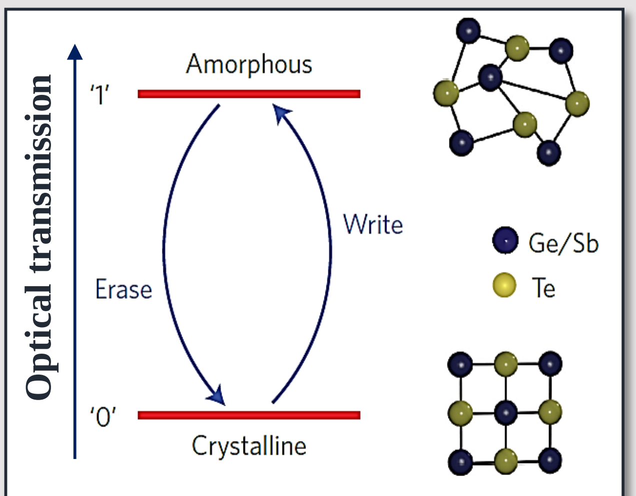

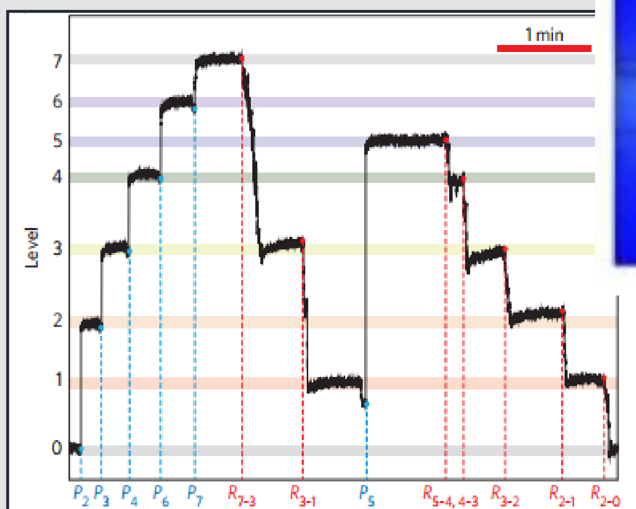

[1] Z. Cheng,. C. Ríos Device-Level Photonic Memories and Logic Applications Using Phase-Change Materials // Advanced Materials. Vol. 30, Is. 32 (2018) P.1802435

Synapse based on the PCM

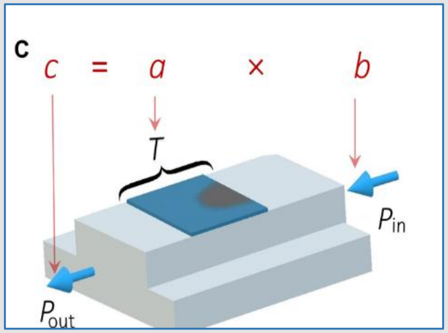

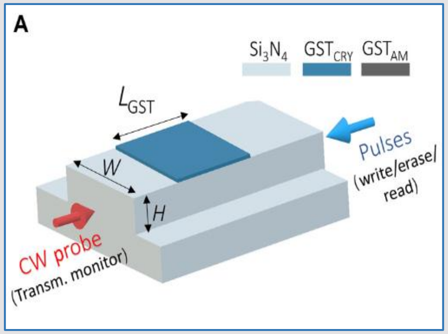

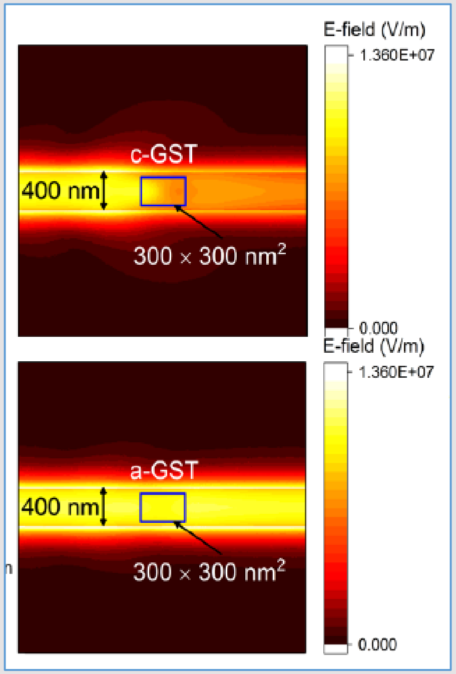

Операция умножения вектора на матрицу в PCM

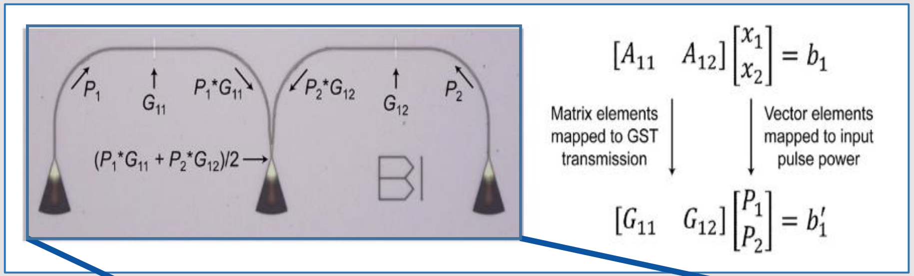

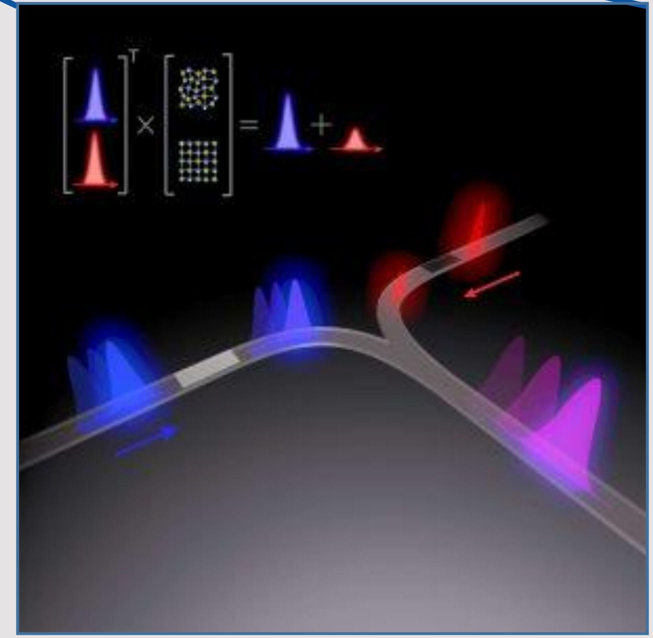

Принцип работы: Обратимое изменение фазового состояния тонкой пленки фазопеременного материала (PCM), покрывающей тонкоплёночный волновод, сопровождается значительными изменением оптических свойств, что позволяет обеспечить управление пропусканием элемента, т.е. интенсивностью проходящего через волновод сигнала.

[1] Rios C. et al. In-memory computing on a photonic platform // Science Advances, 2019. – P. 1–9.

Optical memory (512 бит)

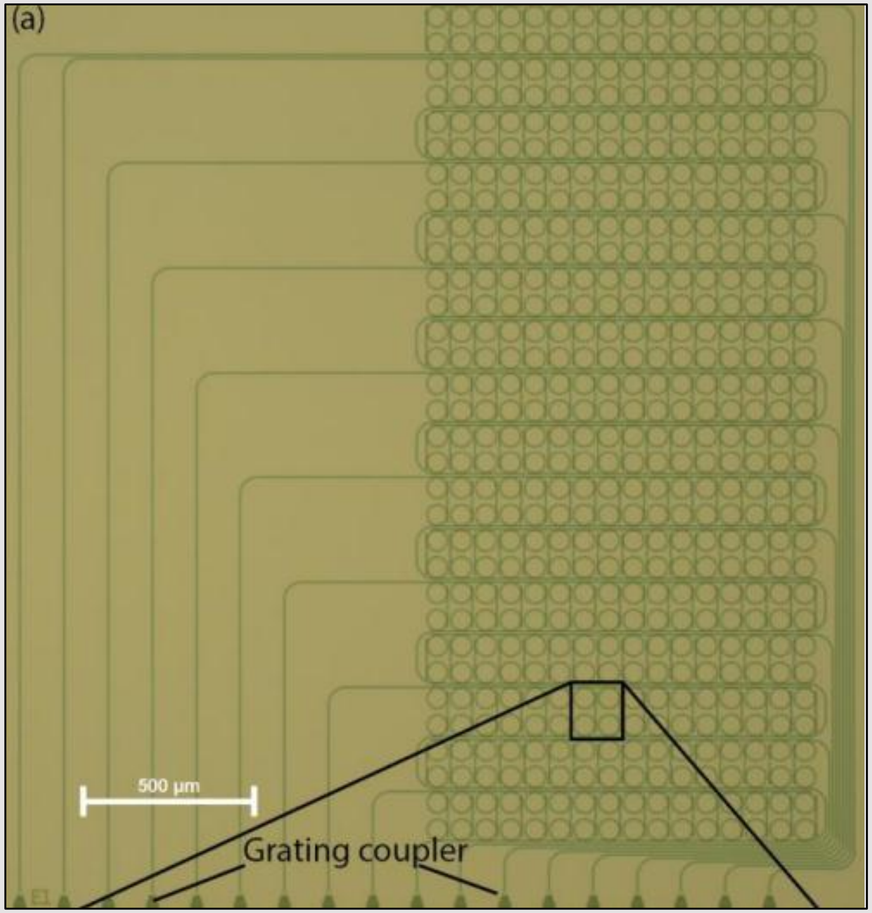

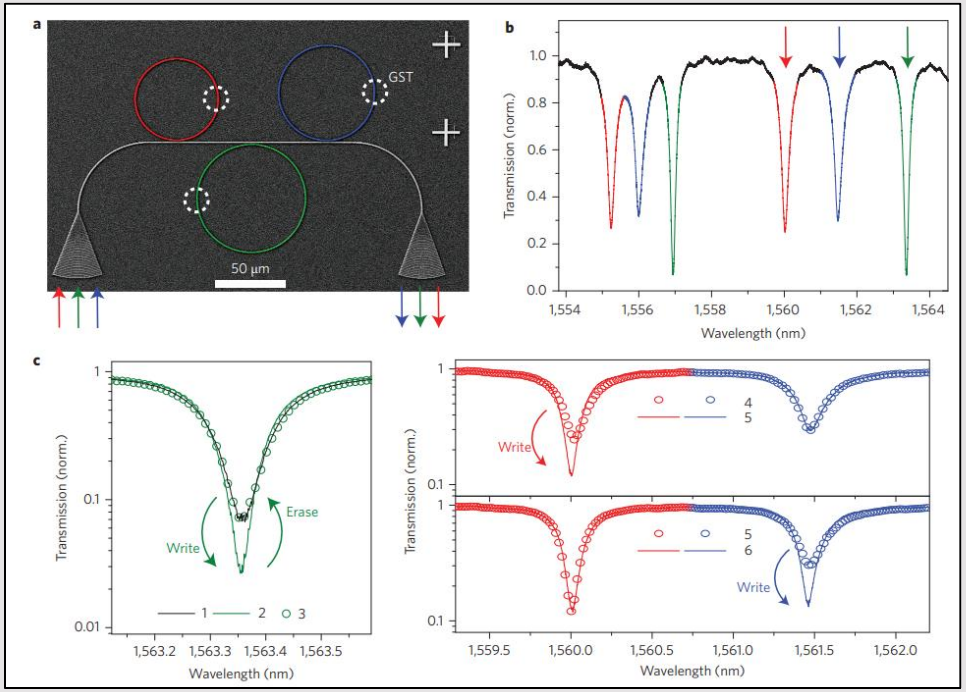

[1] C. Lian, et al. Photonic (computational) memories: tunable nanophotonics for data storage and computing // Nanophotonics 2022. - P. 3823–3854
[2] J. Feldmann, et al. Integrated 256 cell photonic phase-change memory with 512-bit capacity // IEEE J. Selected Topics in Quantum Electron, 2019. - P. 1-7.

An integrated photonic tensor core

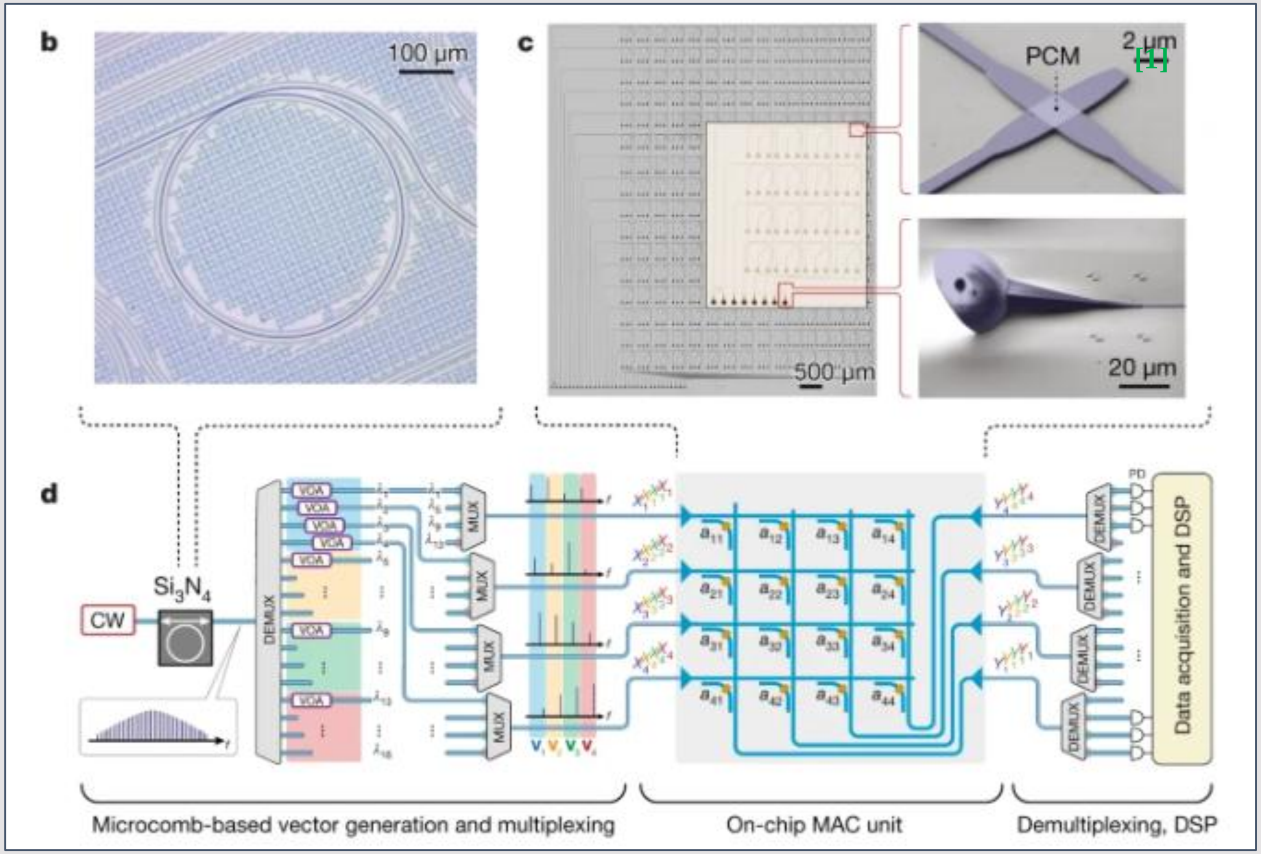

$$\begin{pmatrix} a_{11} & a_{12} & \dots & a_{1j} \\ a_{21} & a_{22} & & a_{2j} \\ \vdots & & & \\ a_{i1} & a_{i2} & & a_{ij} \end{pmatrix}^T \times \begin{pmatrix} X_1 \\ X_2 \\ \vdots \\ X_i \end{pmatrix} = \begin{pmatrix} Y_1 \\ Y_2 \\ \vdots \\ Y_j \end{pmatrix}$$

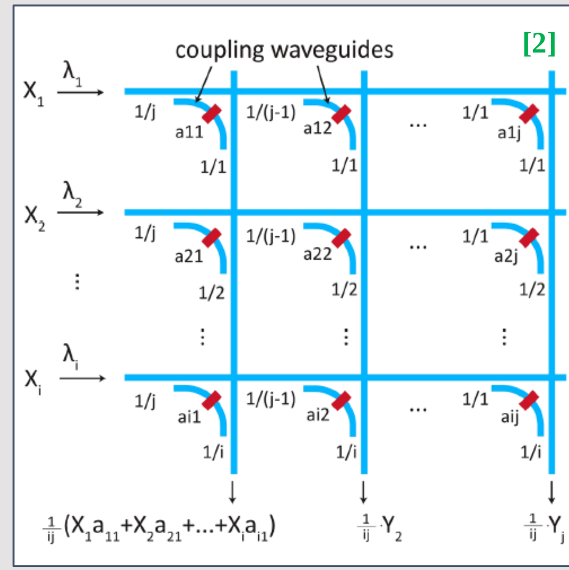

[1] J. Feldmann, et al. Parallel convolutional processing using an integrated photonic tensor core // Nature, 2021. - Vol. 589, P. 52-58.
[2] F. Brückerhoff-Plückelmann, et al. Chalcogenide phase-change devices for neuromorphic photonic computing // Journal of Applied Physics, 2021. - Vol. 129, P. 151103.

Material optimization

Comparison of the various PCMs

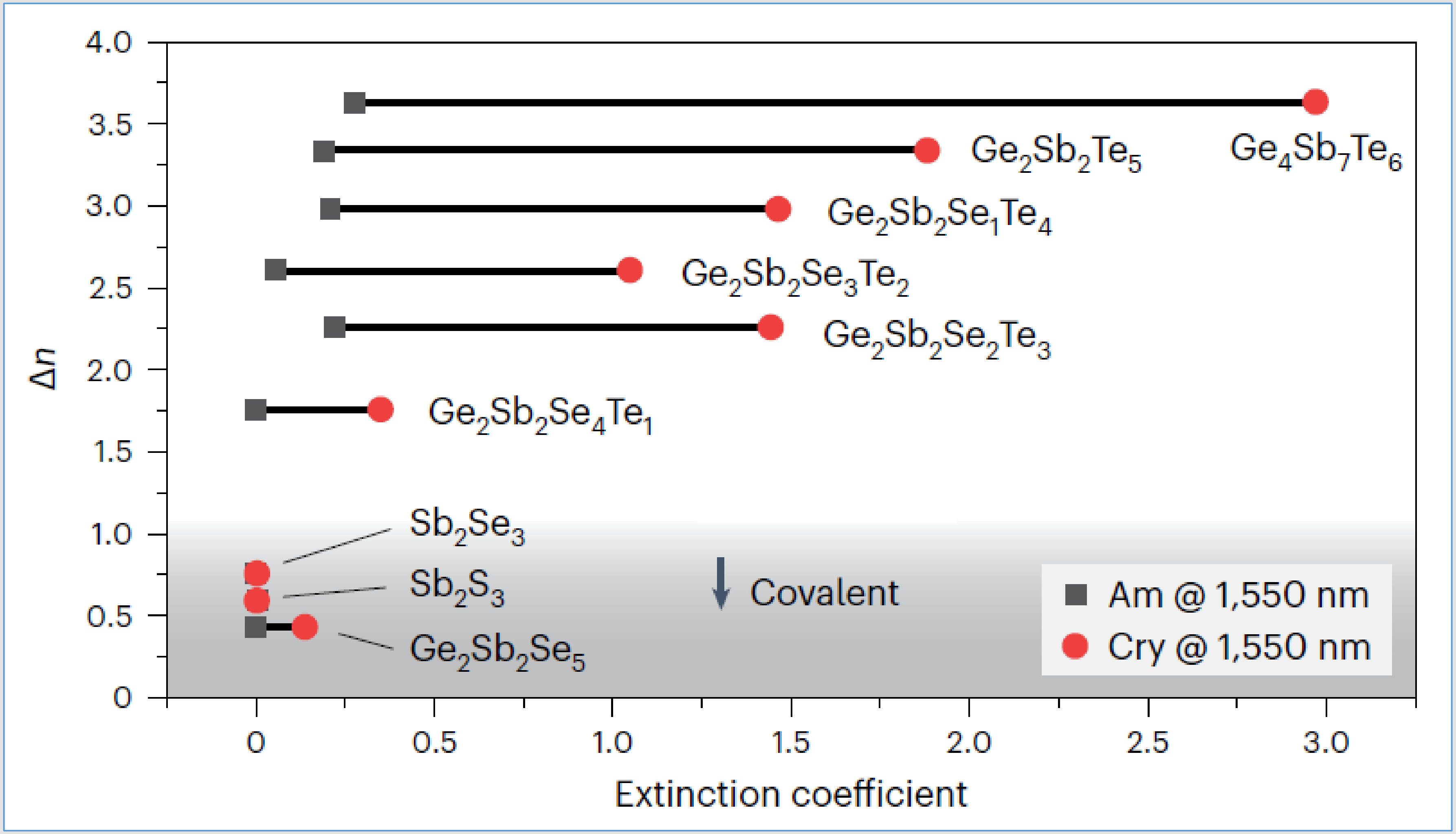

[1] N.Youngblood et al. Integrated optical memristors // Nature Photonics (2023)

Sn doped $Ge_2Sb_2Te_5$ (GST255)

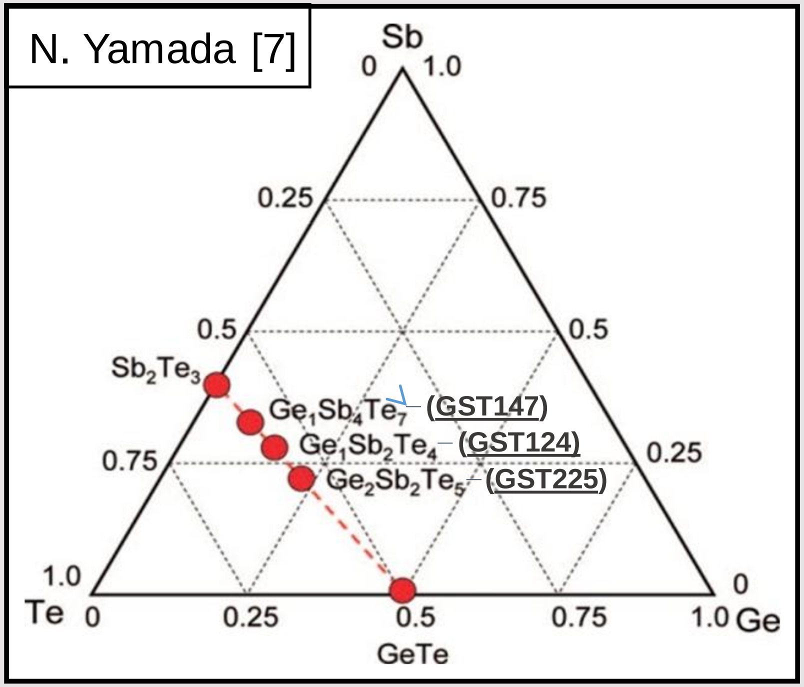

III	IV	V	VI
Al 13 АЛЮМИНИЙ 26,092	Si 14 КРЕМНИЙ 28,086	P 15 ФОСФОР 30,974	S 16 СЕРА 32,064
Ga 31 ГАЛЛИЙ 69,72	Ge 32 ГЕРМАНИЙ 72,59	As 33 МЫШЬЯК 74,922	Se 34 СЕЛЕН 78,96
In 49 ИНДИЙ 114,82	Sn 50 ОЛОВО 118,69	Sb 51 СУРЬМА 121,75	Te 52 ТЕЛЛУР 127,6
Tl 81 ТАЛЛИЙ 204,37	Pb 82 СВИНЕЦ 207,19	Bi 83 ВИСМУТ 208,98	Po 84 ПОЛОНИЙ [210]

Sn and Ge are isomorphic elements

Atomic radii	R_{Ge}=0,128 nm R_{Sn}=0,151 nm
Values of electronegativities	• χ_{Ge}=2,01 • χ_{Sn}=1,96
Bond energy (ΔH^f_{298})	• *402 kJ/mol for Ge-Te* • *319,2 kJ/mol for Sn-Te*

So, we supposed, that in GST225 the replacement of Ge with isovalent Sn occurs according to the mechanism of substitution.

Objectives

Fundamental

Applied

Fundamental task

Properties of as-deposited

Sn-doped $Ge_2Sb_2Te_5$ thin films

Sn doped GST225 (TEV)

Initial bulk alloy	Thin film
$(Ge_2Sb_2Te_5)_{99.5}Sn_{0.5}$	$(Ge_2Sb_2Te_5)_{99.4}Sn_{0.6}$
$(Ge_2Sb_2Te_5)_{99}Sn_1$	$(Ge_2Sb_2Te_5)_{99.1}Sn_{0.9}$
$(Ge_2Sb_2Te_5)_{97}Sn_3$	$(Ge_2Sb_2Te_5)_{96.2}Sn_{3.8}$

- The peak D has disappeared at 300 cm^{-1}, while peaks B and C have shifted to lower wavenumbers for 0,5 wt.% Sn (to 117 and 145 cm^{-1}, respectively).
- This shift is even more pronounced (108 and 140 cm^{-1}) for 3 wt. % tin concentration (see also peaks of B2 and C2).

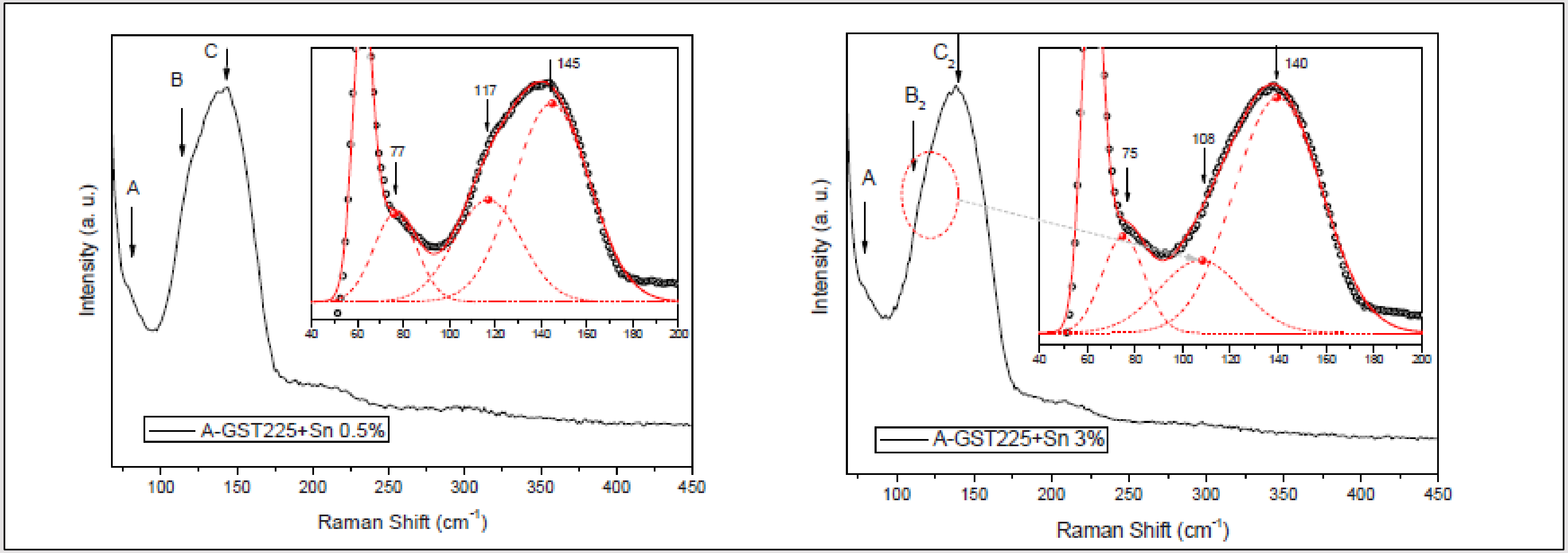

Raman spectra of a-GST225 thin films doped Sn.

MS vs TEV

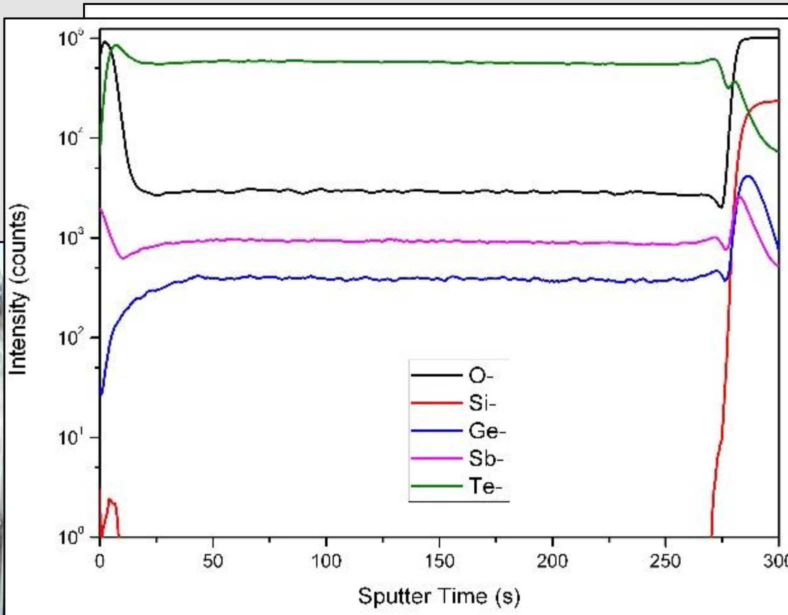

thesis
gh pu … ver
melt i … amp
he am … 10-
ently … xin

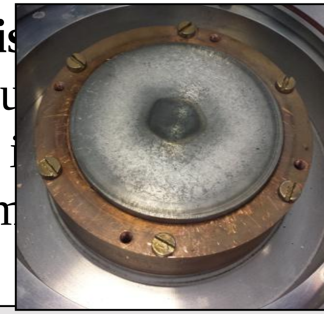

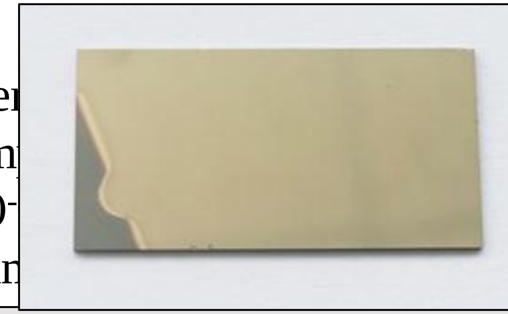

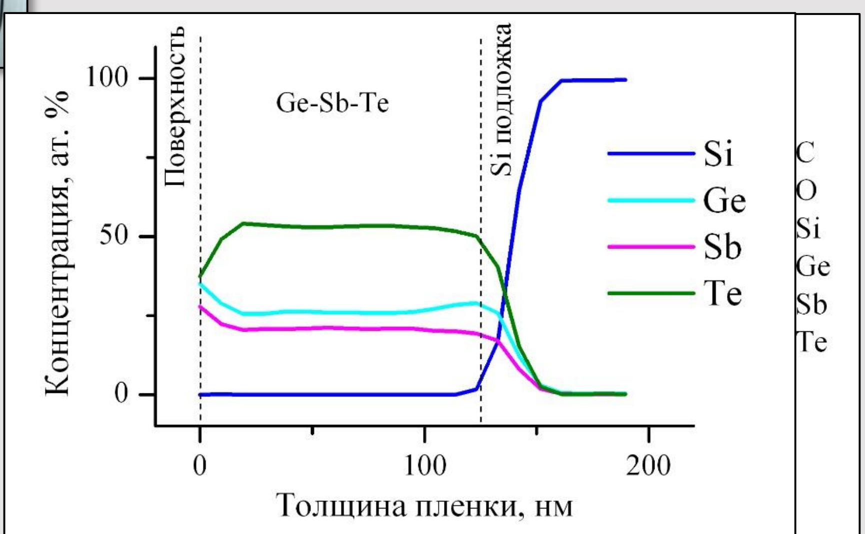

Thin films of $Ge_2Sb_2Te_5$
were prepared by two deposition methods:

TEV 1. Thermal evaporation in vacuum.

Residual pressure in the chamber was 10^{-4} Pa. The maximum temperature during evaporation was not more than 630 °C, substrate temperature < 50°C.

MS 2. Magnetron sputtering.

Monolithic polycrystalline $Ge_2Sb_2Te_5$ (5N) was used for DC sputtering. The pressure of Ar during the process was $2{\cdot}10^{-3}$ Torr.

Sn ion implantation

The Sn ion implantation was done on the Multipurpose Test Bench (MTB) at “Kurchatov Institute”- ITEP

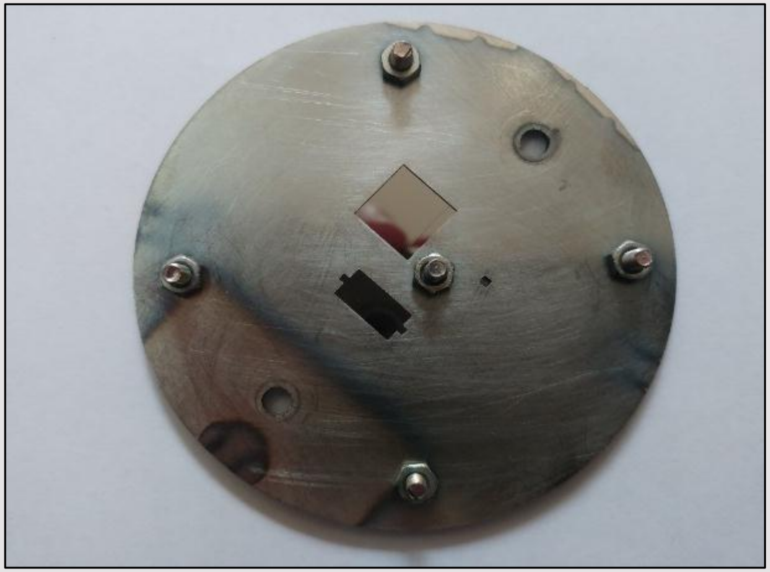

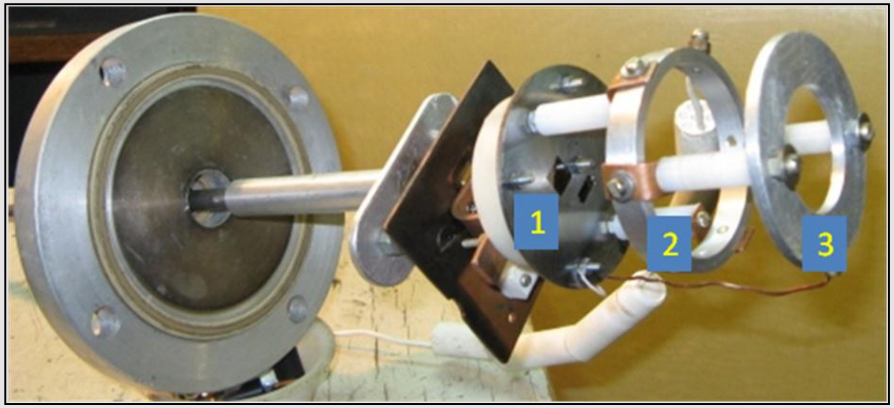

Combined target where 1 – target, 2 – suppressor ring, 3 – defending ring

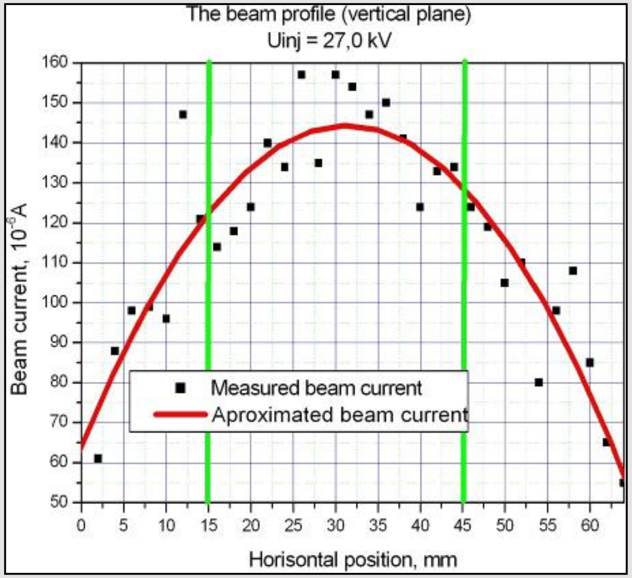

The beam`s profile

$(Ge_2Sb_2Te_5)_{1-x}Sn_x$

The uniformity of the elemental distributions across the film thicknesses was determined by Time-of-Flight secondary ion mass and Auger electron spectrometries.

Dose, p/cm²	0.14·10¹⁴	0.7·10¹⁴	1.4·10¹⁴	2.8·10¹⁴	7·10¹⁴
Sn, at.%	0.1	0.5	1	2	5

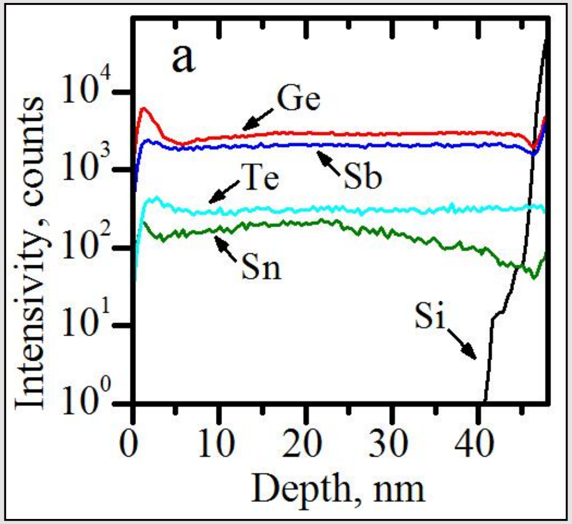

Time-of-Flight secondary ion mass spectrometry

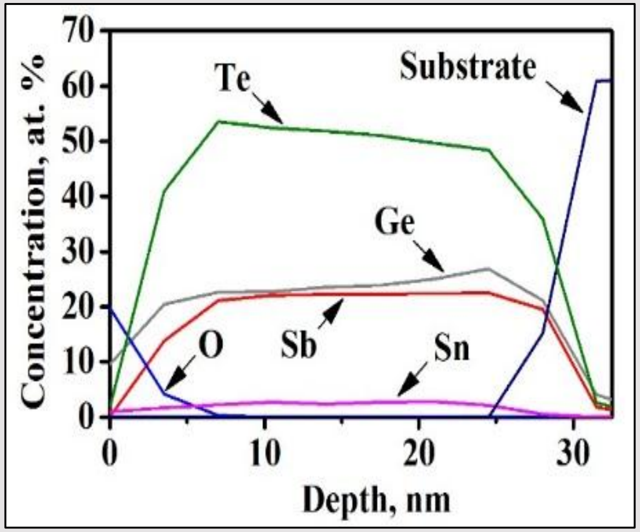

Auger electron spectroscopy

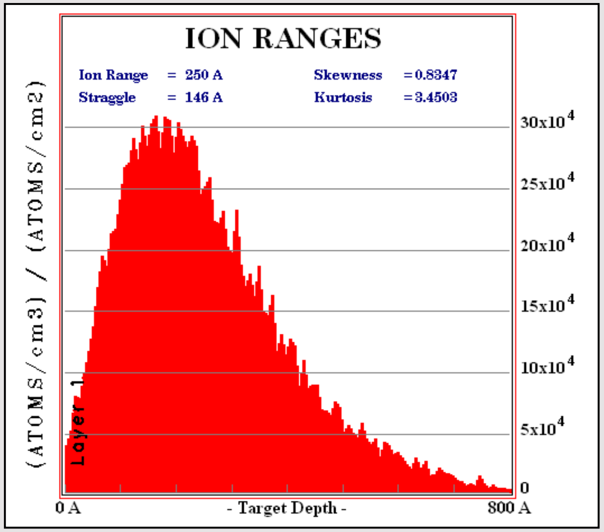

The Bragg peak of Sn ions (Sn^+ and Sn^{2+}) in the GST225 film

---

Results of Auger electron spectrometry showed that $7 \cdot 10^{14}$ and $2.8 \cdot 10^{14}$ p/cm² fluences provide the average Sn concentration 5 and 2 at. % in GST225, which corresponds to the calculated concentrations.

X-ray Photoelectron Spectroscopy

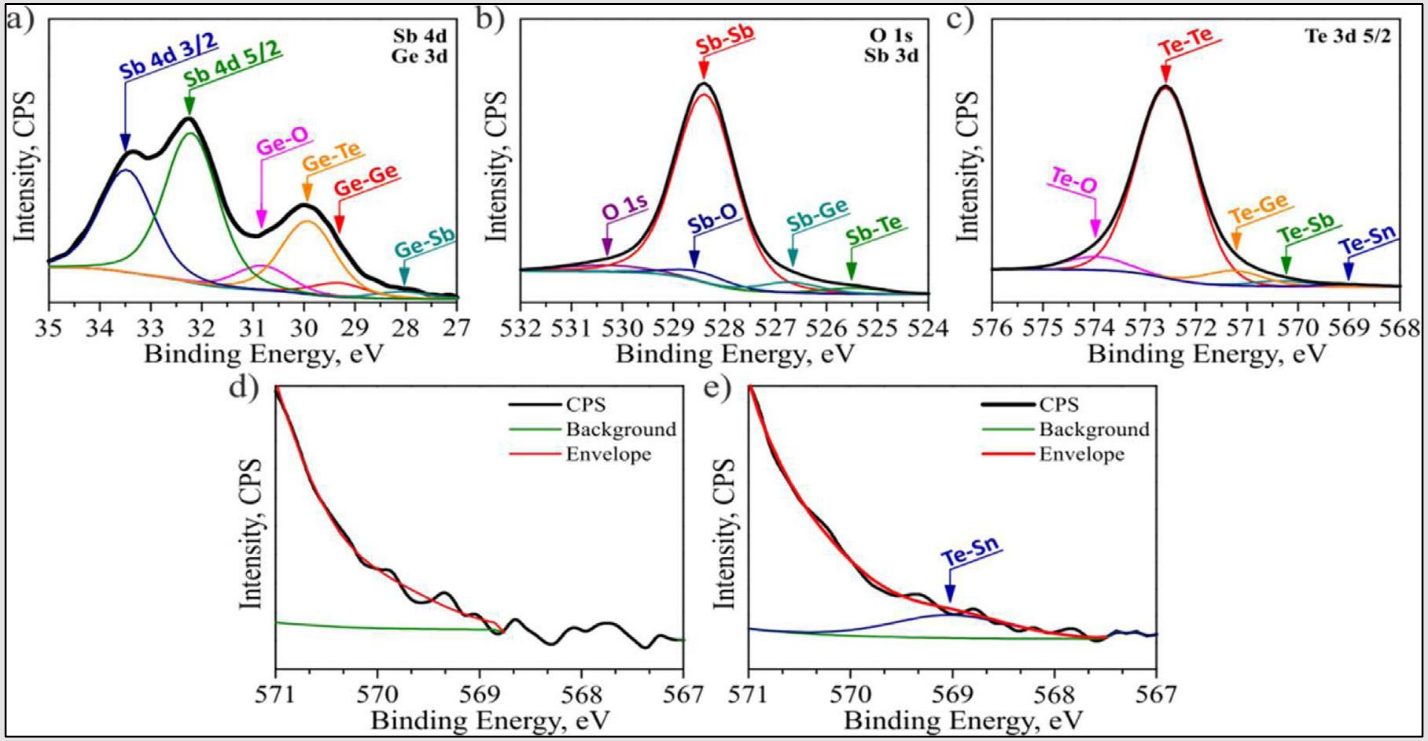

So, tin ion implantation in GST225 films leads to the effective replacement of the Ge by Sn.

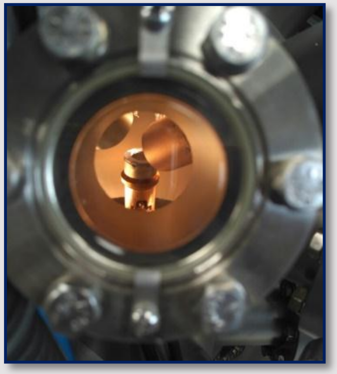

- Samples were preliminarily etched by Argon-ion plasma in order to achieve clean surface as samples were exposed to air.
- During measurements, samples were cooled down to liquid Nitrogen temperature to avoid any heating originating from X-ray source exposure.

Electrical properties

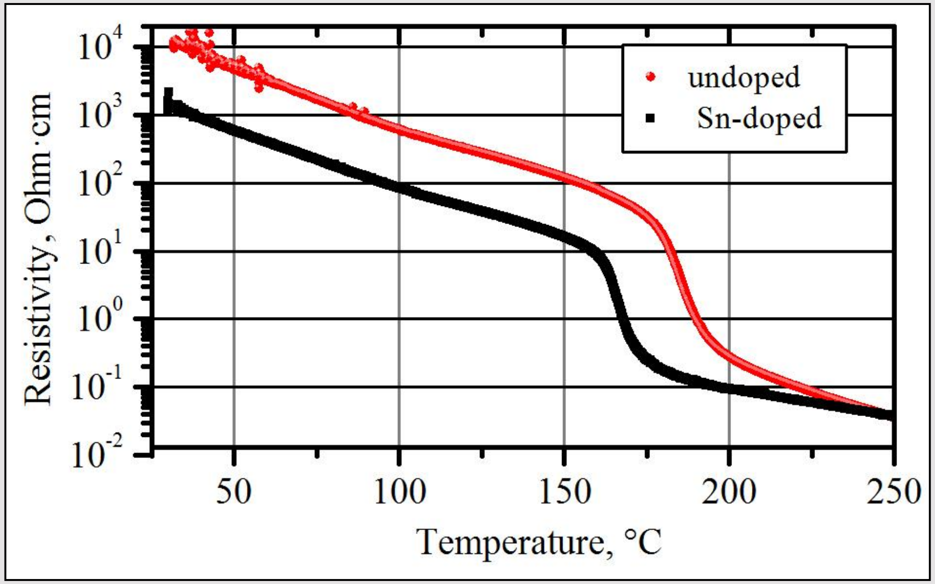

T_{set}, °C	T_{end}, °C	ρ_{set}, Ω·cm	E_a, eV
undoped GST thin film			
176.7	193.9	$4.58 \cdot 10^3$	0.43
Sn-doped GST thin film			
161.1	173.1	$5.80 \cdot 10^2$	0.42

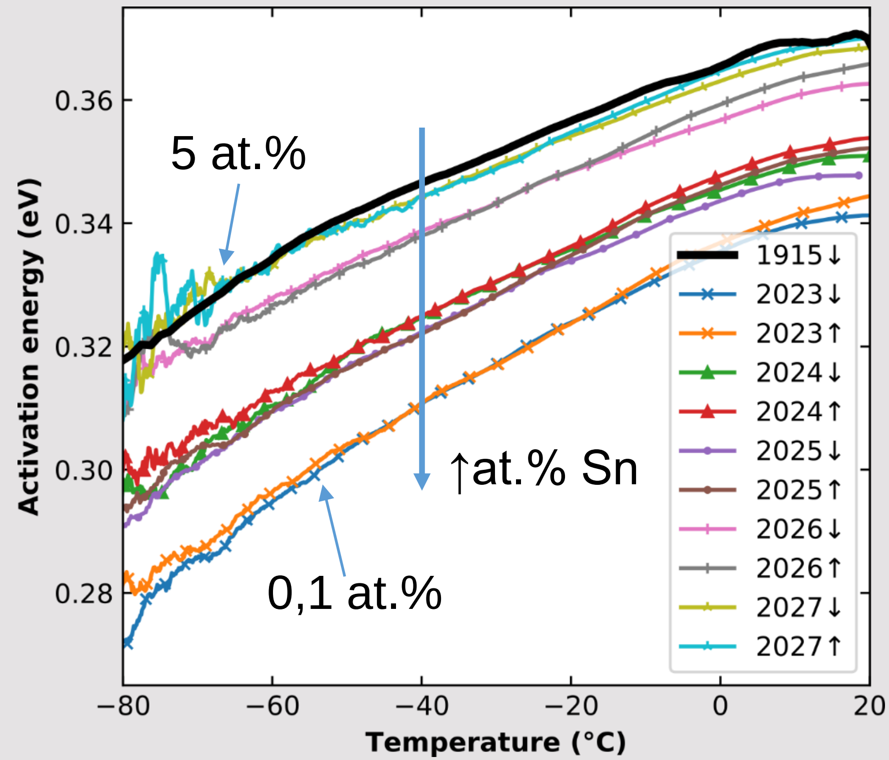

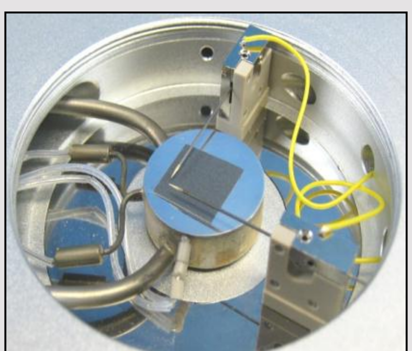

The HFS600E-PB4/PB2 stage consists of a pure silver heating/cooling block; heating element wire, stainless steel cooling tube, platinum temperature sensor and electrical probe.

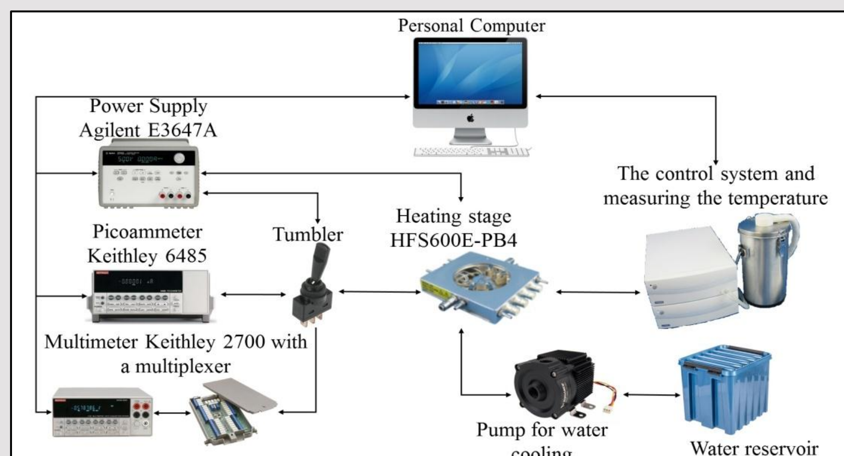

Optical properties

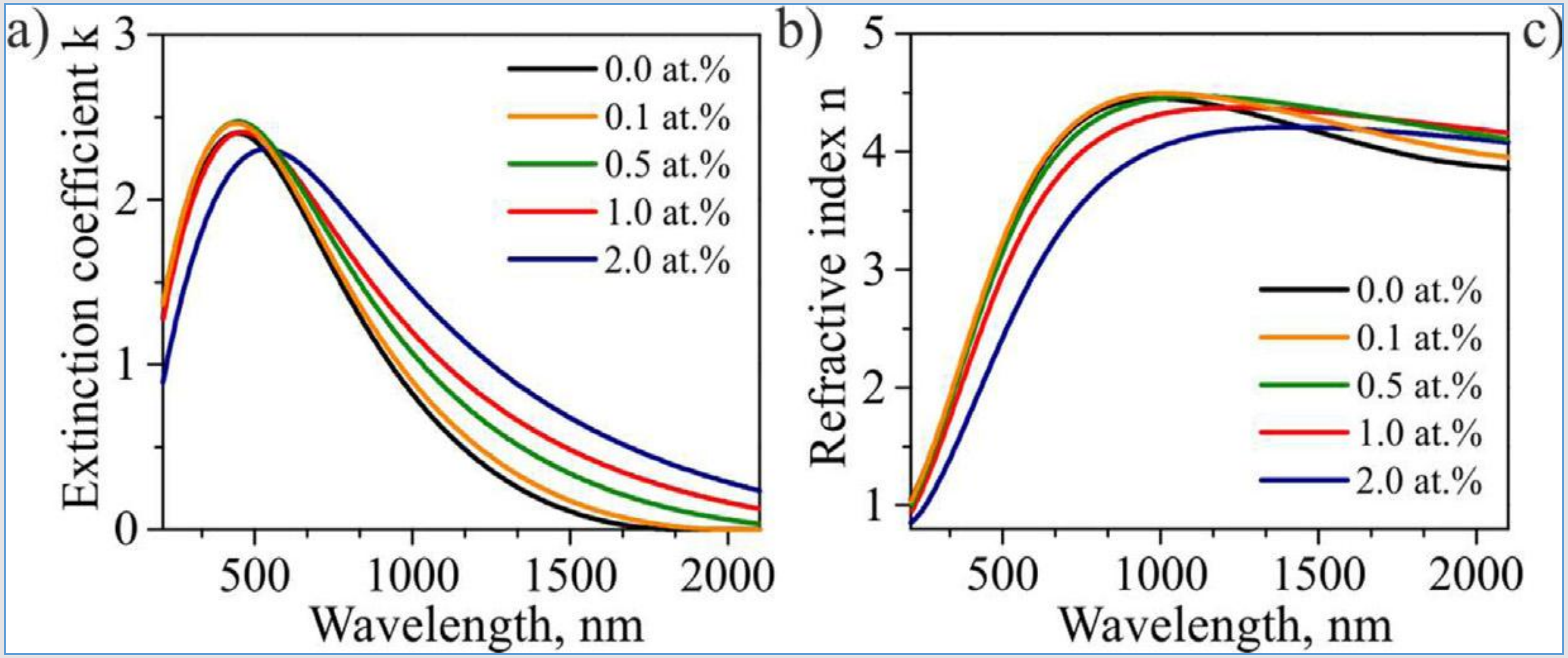

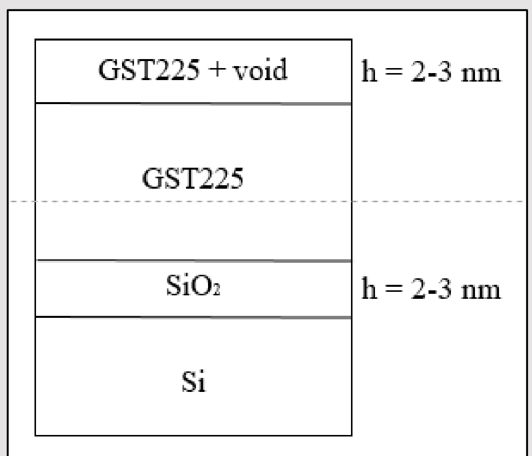

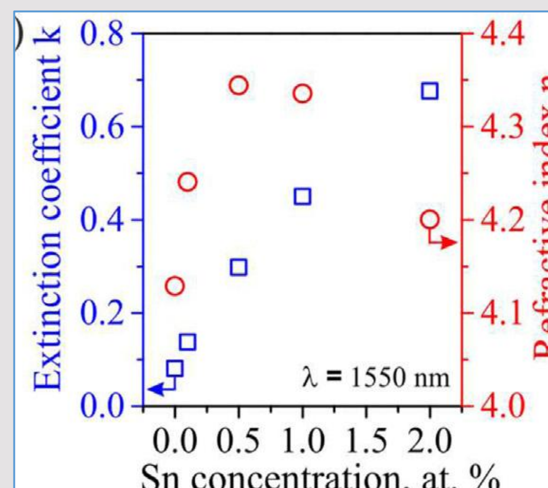

Surface oxidation

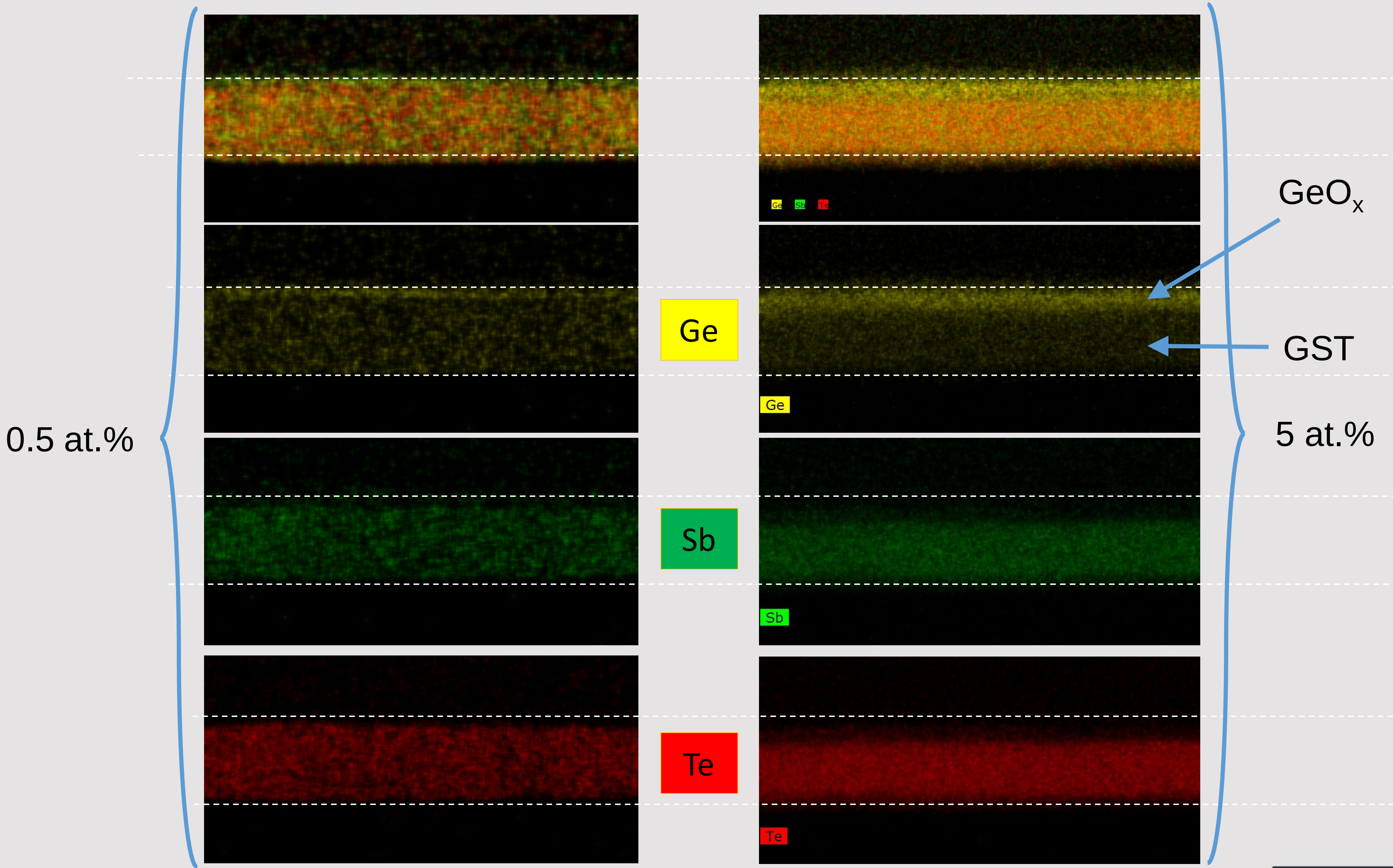

Elemental distributions

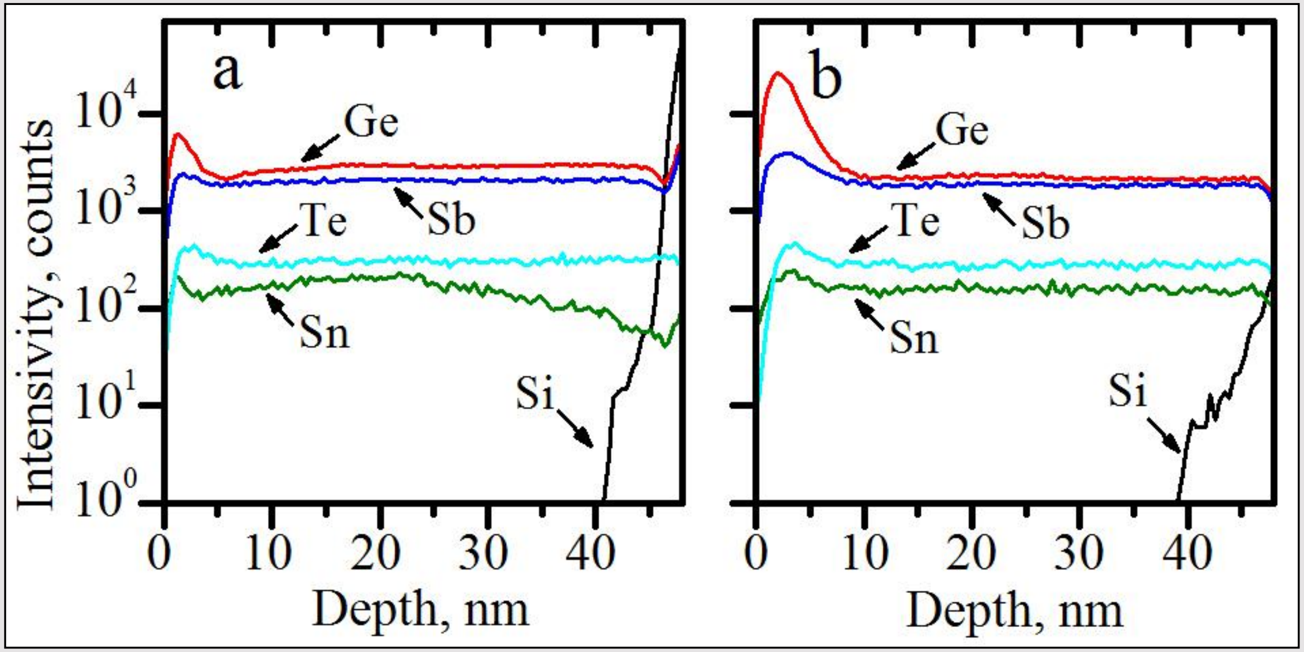

Elemental distributions along the film thicknesses according to TOF-SIMS for Sn-doped GST225 thin films: a – before annealing; b – after annealing at 400 °C.

Laser irradiation

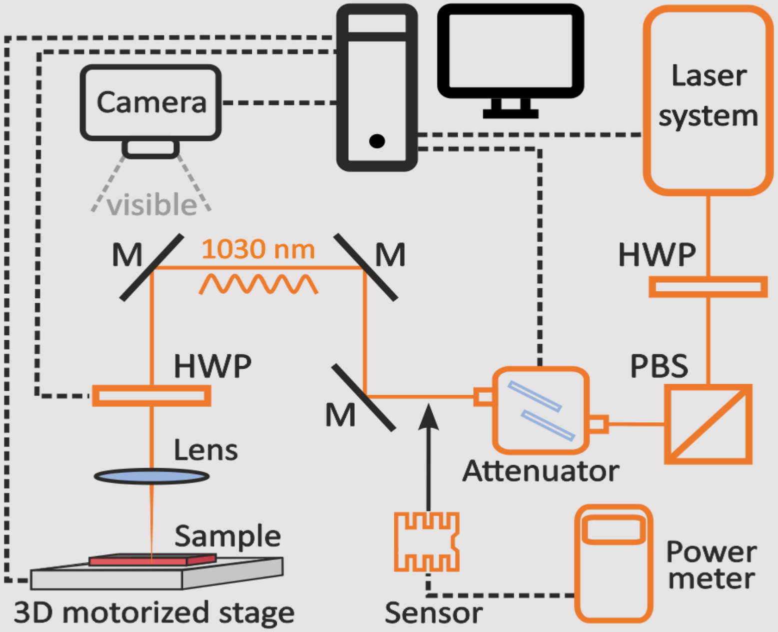

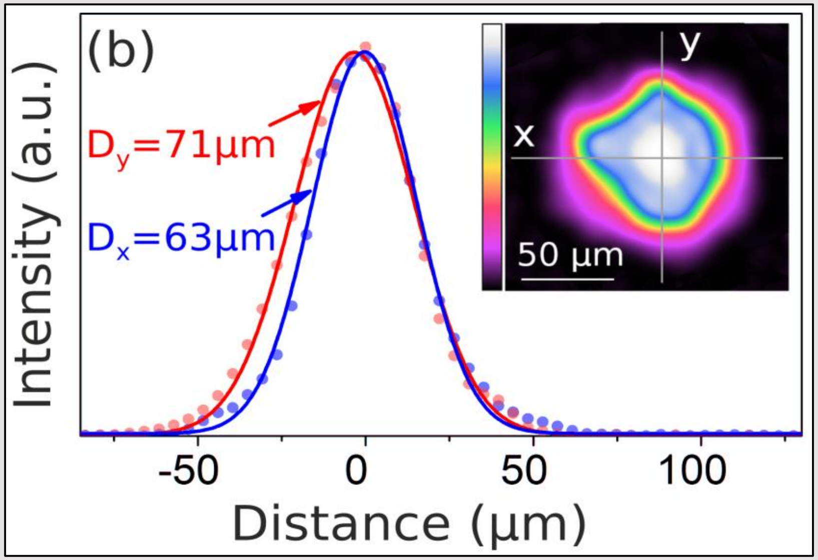

Laser Pharos SP (Yb:KGW, 6 W)
Wavelength: 1030 nm
Repetition rate: 1 kHz – 1 MHz (200 kHz)
Duration: 180 fs-8 ps
Diameter ($1/e^2$): 65 µm
Number of pulses: 500

Air-bearing translational XYZ stage AeroTech A3200
CCD camera Spiricon SP620U
HWP is the half wave plat
PBS is the polarization beam splitter

Raman spectroscopy

as-deposited (1) crystallized (2) re-amorphized (3)

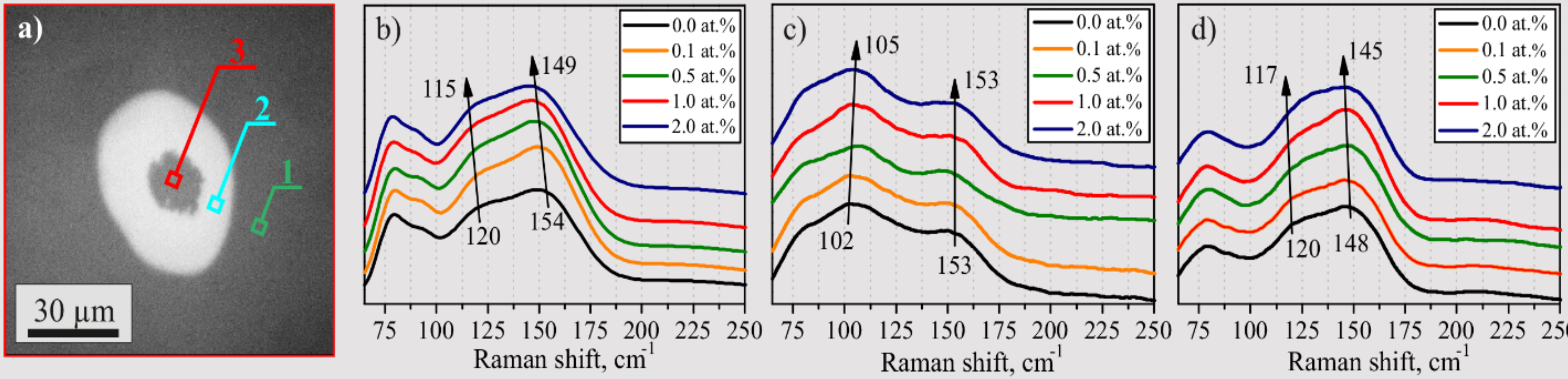

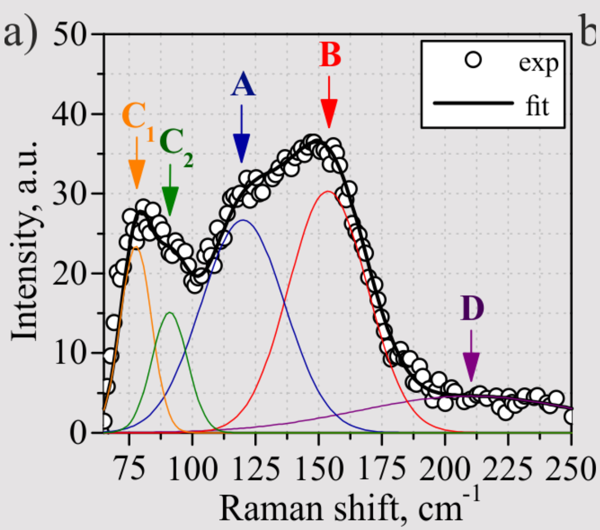

b

Sn, at. %	C_1		C_2		A		B		D	
	PP(cm^{-1})	FWHM	PP(cm^{-1})	FWHM	PP (cm^{-1})	FWHM	PP (cm^{-1})	FWHM	PP (cm^{-1})	FWHM
0.0	78	7.3	91	8.3	120	19.5	154	18.3	210	52.0
0.1	78	7.3	91	8.3	120	19.4	154	18.2	210	52.0
0.5	78	7.3	90	8.3	119	19.4	152	18.8	210	52.0
1.0	77	7.3	89	8.3	117	19.8	151	18.6	210	52.0
2.0	77	7.0	89	8.3	115	19.0	149	19.0	210	52.0

Threshold energies

F_{max} of 5.1 and 12.8 mJ/cm^2.

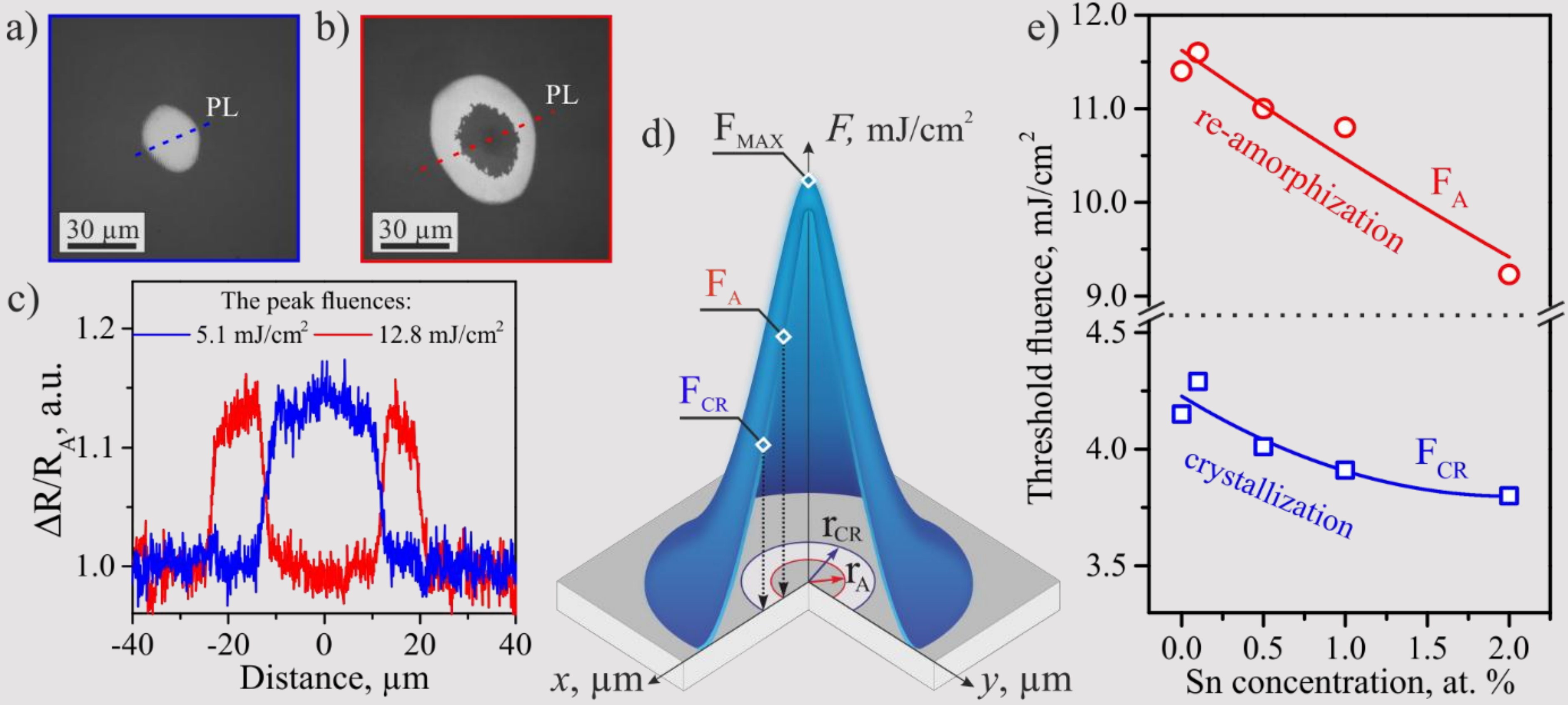

The threshold energy of crystallization and amorphization processes, due to the pulse laser influence, noticeably decreased from 4.2 to 3.8 mJ/cm^2 (9 %) and from 11.4 to 9.2 mJ/cm^2 (19 %), respectively.

Applied task

Demonstration of the possibility of using Sn-doped GST225 to provide reversible multilevel switching in the integrated nanophotonic devices

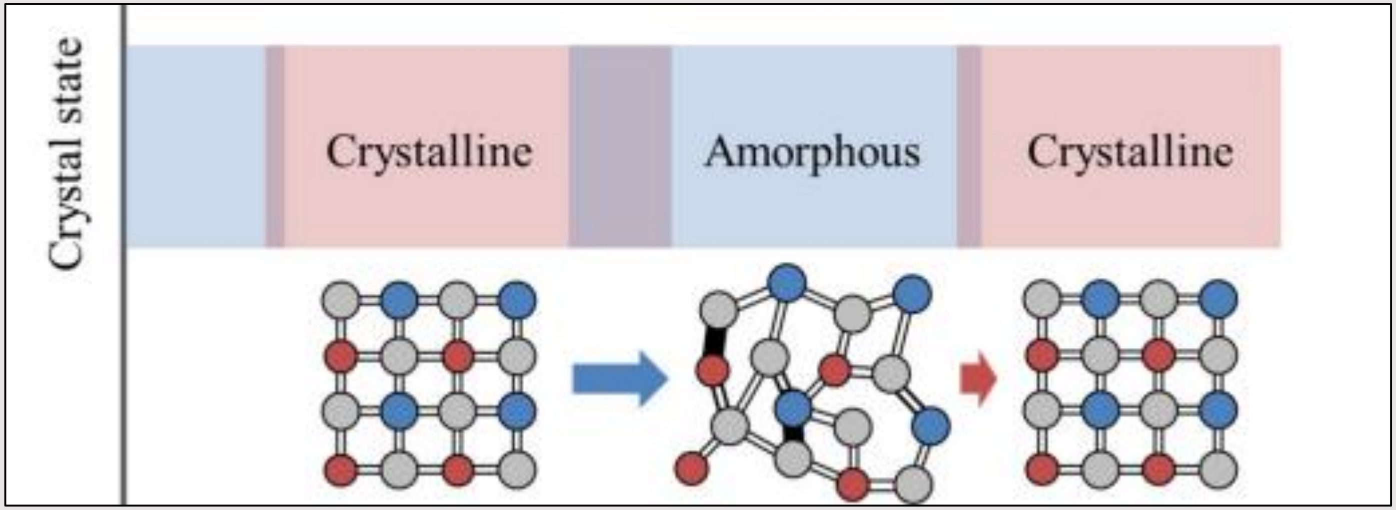

Fabrication process

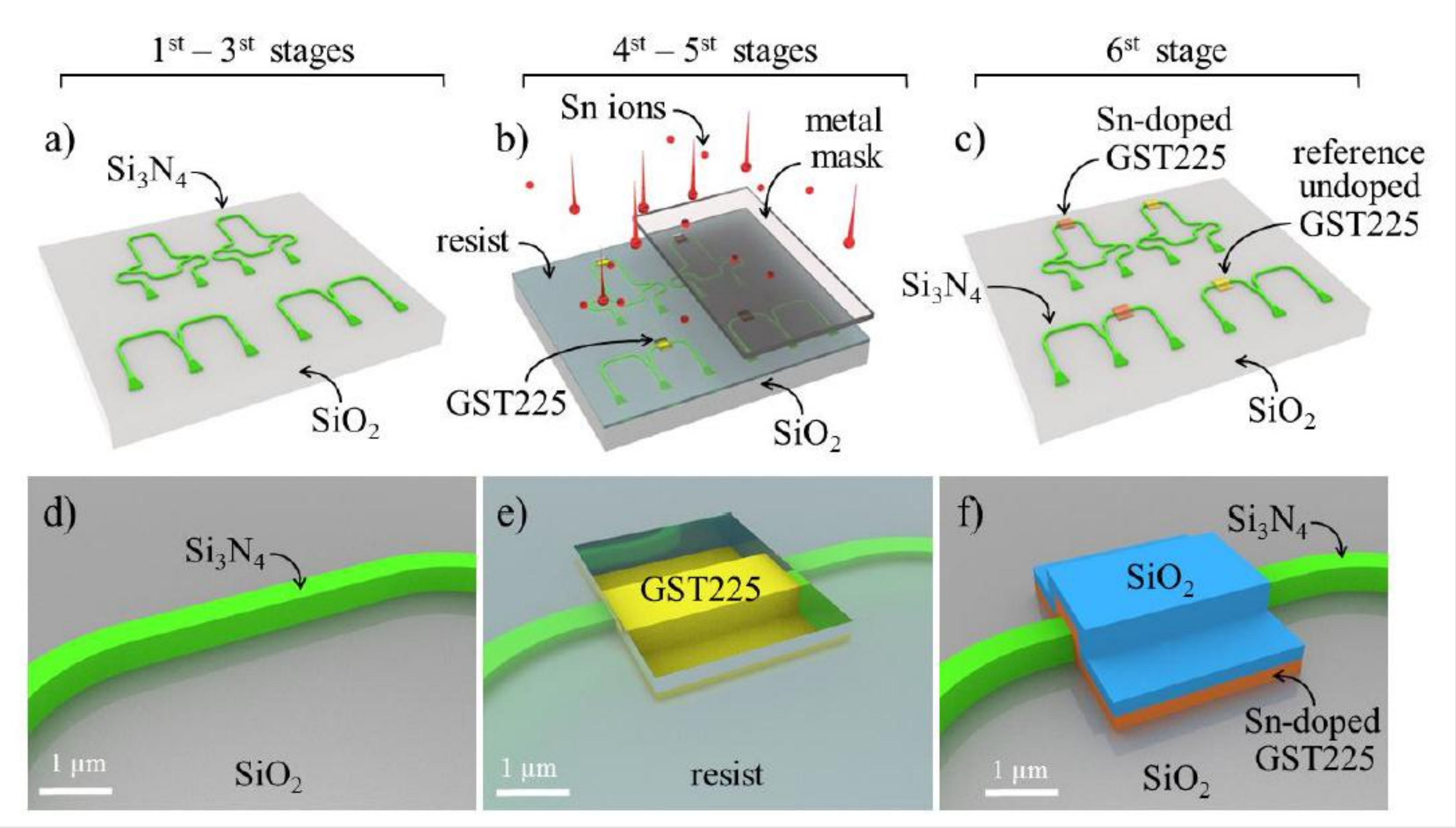

Nanophotonic devices

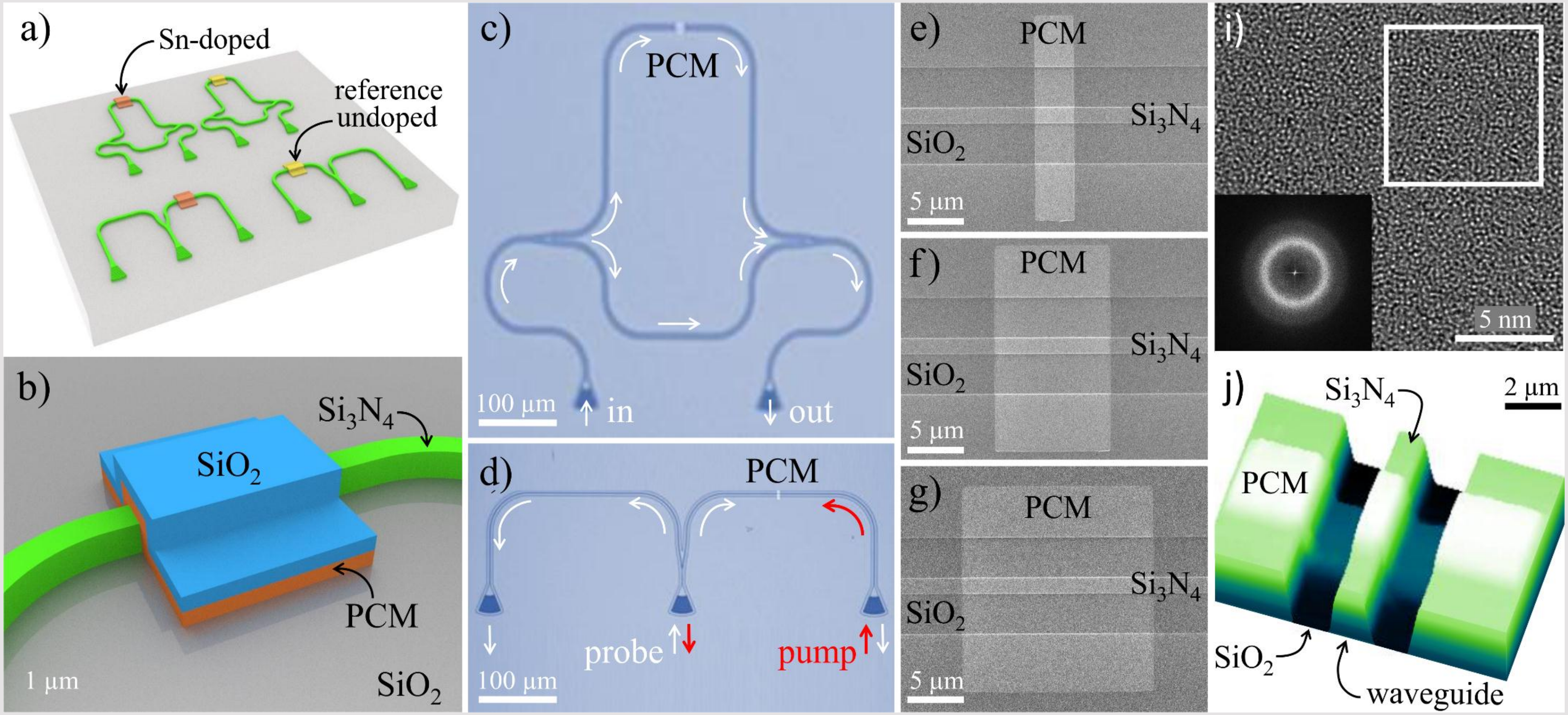

The schematic view of two types of on-chip nanophotonic devices: Mach-Zehnder interferometers and balanced splitters (b) The schematic of PCM cell. (c, d) Optical micrographs of the fabricated MZI and BS (e-g) SEM images of PCM cells with different lengths. (i) TEM image and Fourier transform pattern (insets) for amorphous GST225.(j) Morphology of the one of the fabricated PCM cells.

---

[1] S. Kozyukhin, et al. Laser-induced modification and formation of periodic surface structures (ripples) of amorphous GST225 phase change materials // Optics and Laser Technology 113 (2019) 87–94

[2] S. Kozyukhin and et al. Specific Features of Formation of Laser-Induced Periodic Surface Structures on $Ge_2Sb_2Te_5$ Amorphous Thin Films under Illumination by Femtosecond Laser Pulses // PSS:B 257 (2020) P. 1900617

Absorption coefficient

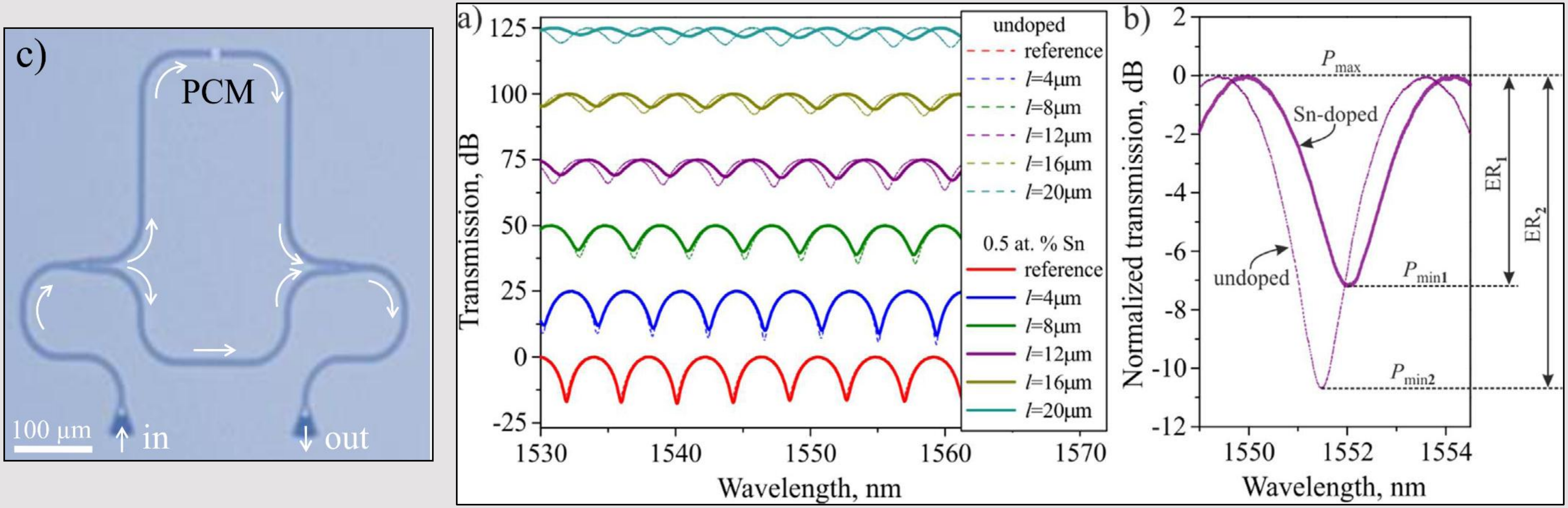

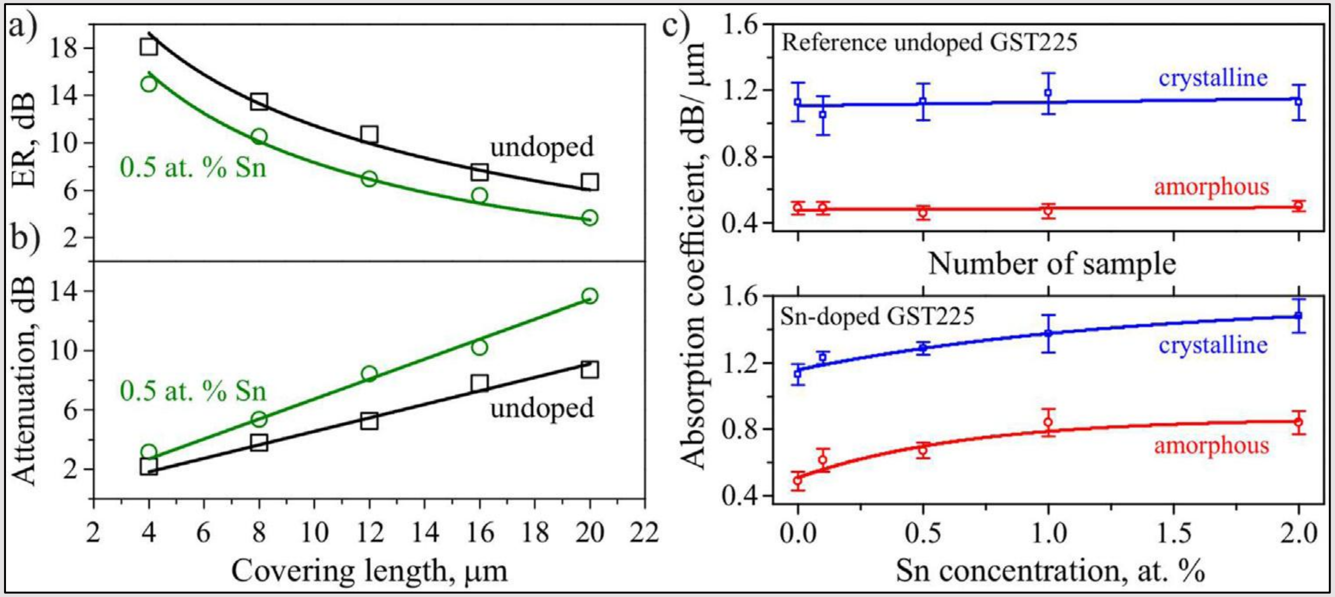

Cell size

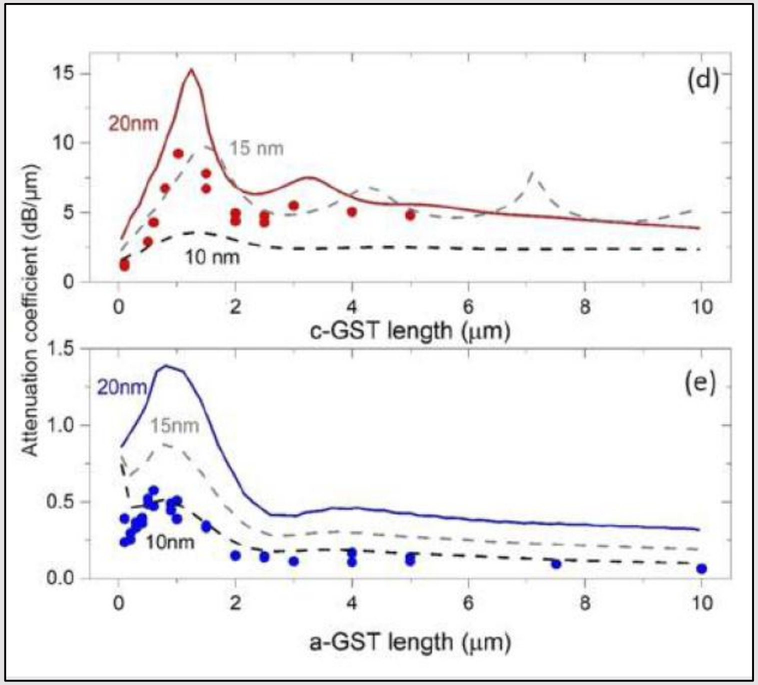

(d)
20nm
15 nm
10 nm
Attenuation coefficient (dB/μm)
c-GST length (μm)
(e)
20nm
15nm
10nm
a-GST length (μm)

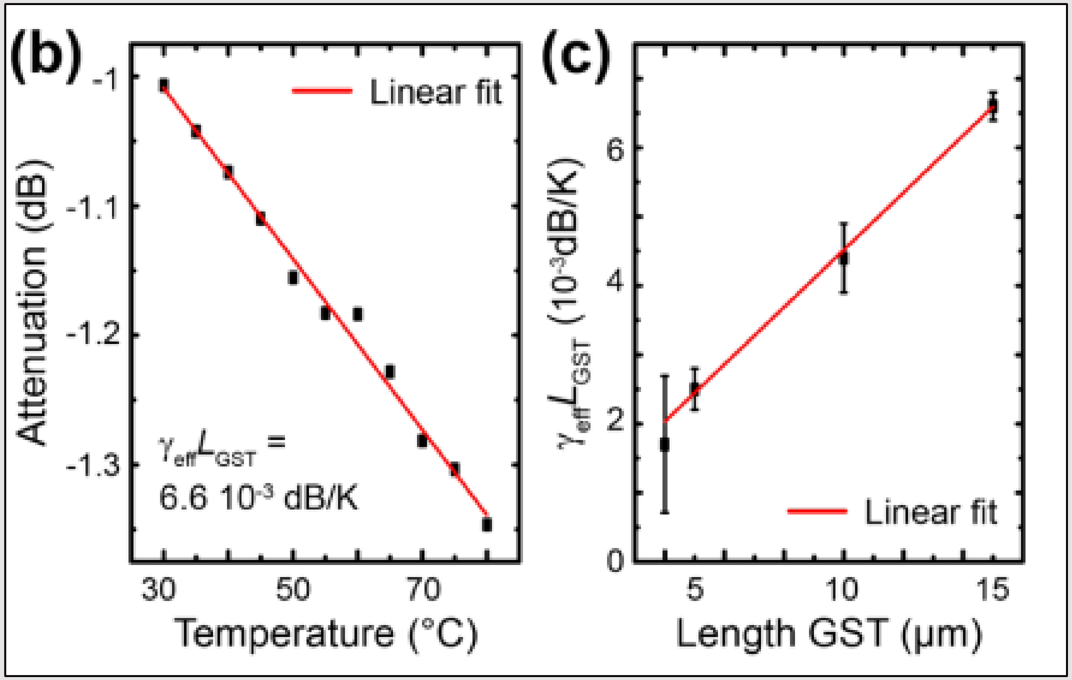

(b)
Linear fit
Attenuation (dB)
$\gamma_{eff}L_{GST}$ =
6.6 10^{-3} dB/K
Temperature (°C)
(c)
$\gamma_{eff}L_{GST}$ (10^{-3}dB/K)
Linear fit
Length GST (μm)

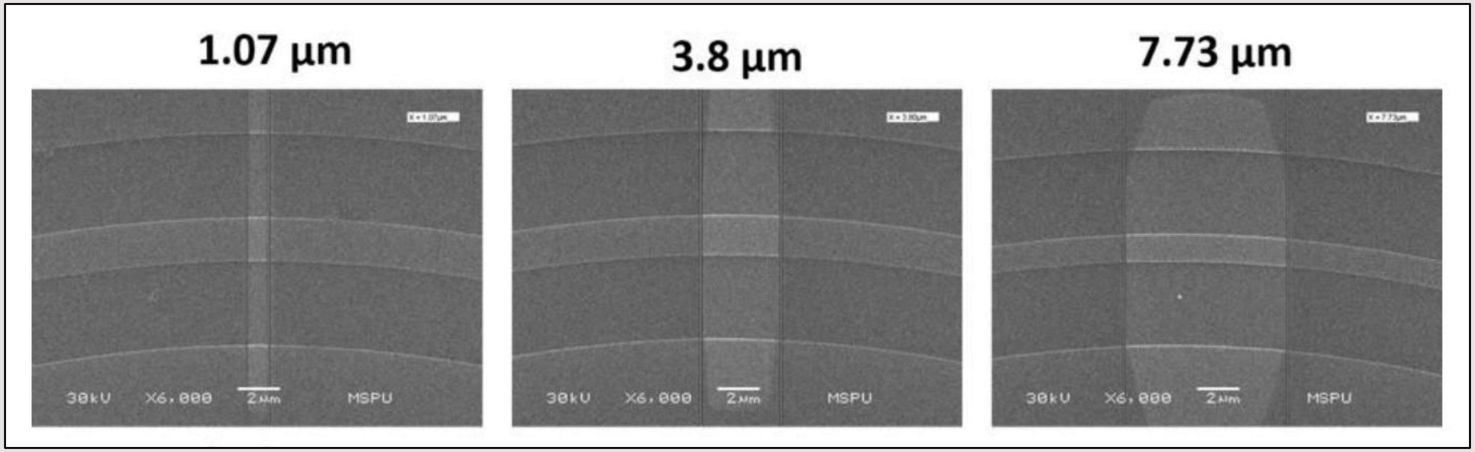

1.07 μm
3.8 μm
7.73 μm
30kV X6,000 2μm MSPU
30kV X6,000 2μm MSPU
30kV X6,000 2μm MSPU

Size effect

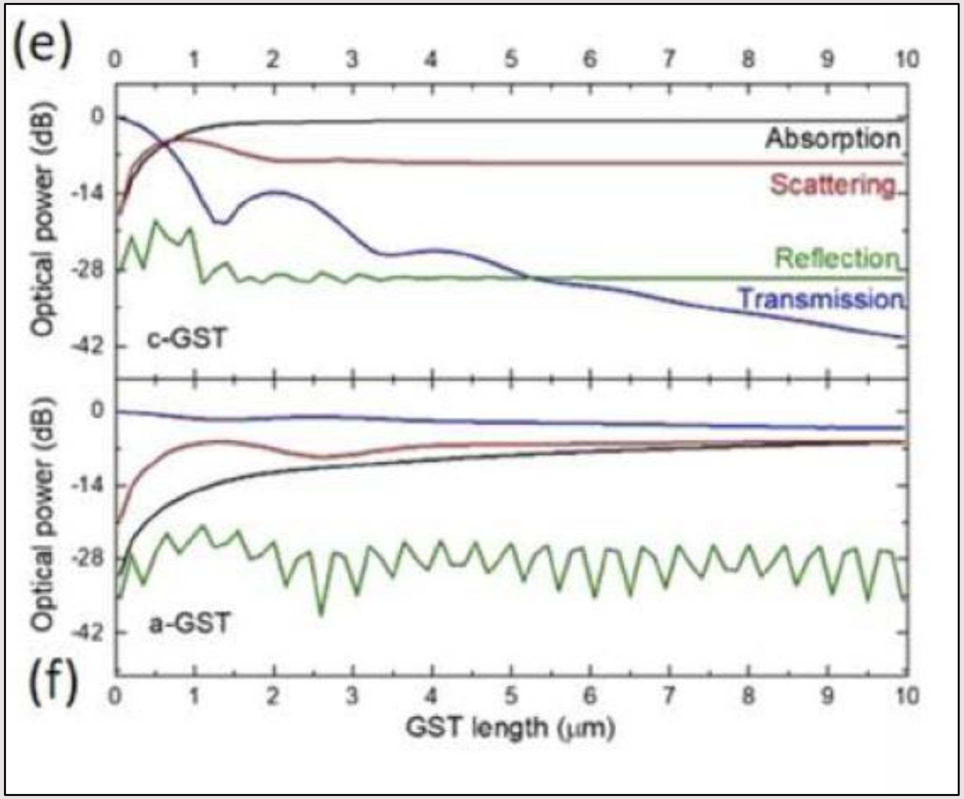

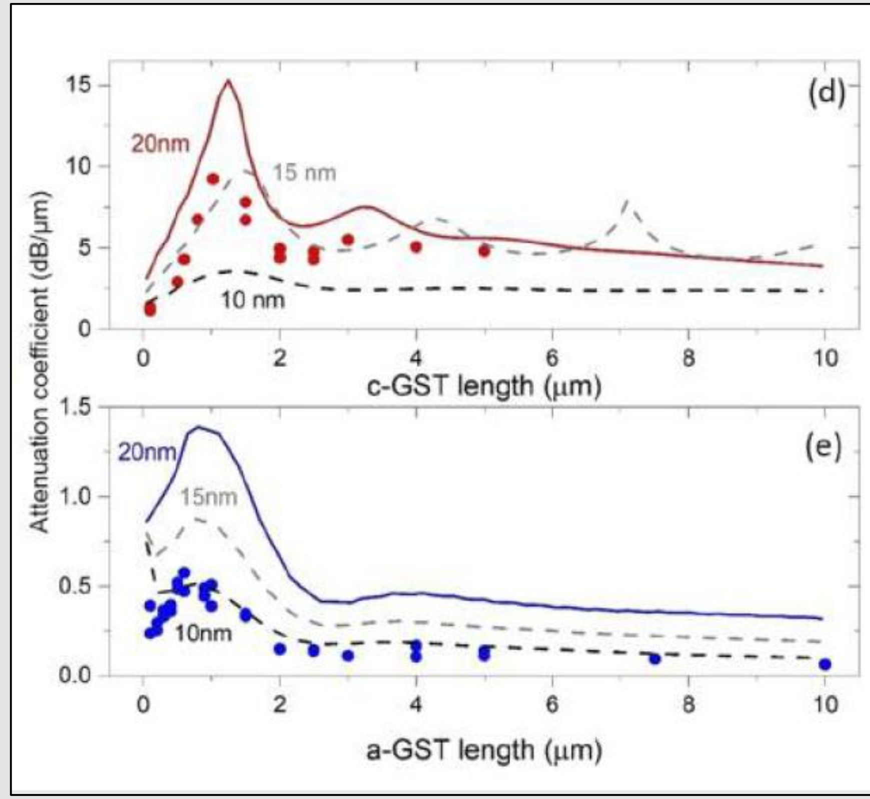

FIG. 5. (a) Optical transmission spectrum of the ORR without any GST (blue) and with the a-GST cell (black) measured in the C-range; (b) enlarged image of the optical transmission spectrum of ORR, before (black) and after a-GST deposition (blue) near the wavelength of 1.55 μm. The red line shows the Lorentz fit. The corresponding values of the peak wavelength and the full width at half maximum before (λ_b, w_b) and after (λ_a, w_a) GST deposition are marked. (d) and (e) Dependence of the attenuation coefficient on the length of the a-GST and c-GST cells. The points are experimentally measured and calculated the data according to Eq. (1). The lines are the data of the 3D numerical calculation for films of different thicknesses: 20 nm (red solid line for c-GST and blue solid line for a-GST), 15 nm (gray dashed line), and 10 nm (black dashed line).

Multilevel reversible recording

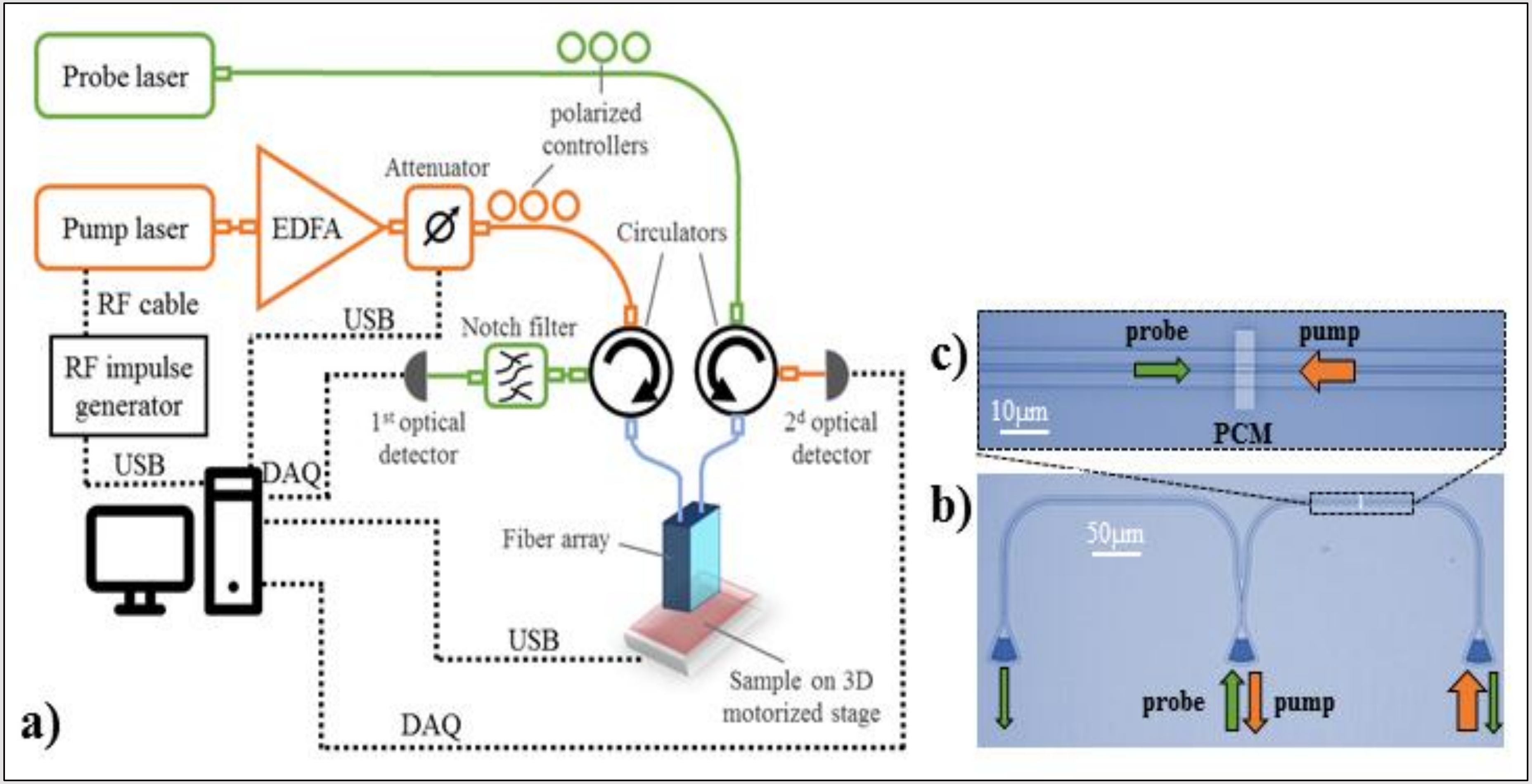

Schematic view of the experimental setup for the pump-probe measurements and the optical image of the fabricated balance spliter. The arrows show the direction of the probe (green) and pump (orange) signals.

[1] S. Kozyukhin, et al. Laser-induced modification and formation of periodic surface structures (ripples) of amorphous GST225 phase change materials // Optics and Laser Technology 113 (2019) 87–94

[2] S. Kozyukhin and et al. Specific Features of Formation of Laser-Induced Periodic Surface Structures on $Ge_2Sb_2Te_5$ Amorphous Thin Films under Illumination by Femtosecond Laser Pulses // PSS:B 257 (2020) P. 1900617

Multilevel reversible recording

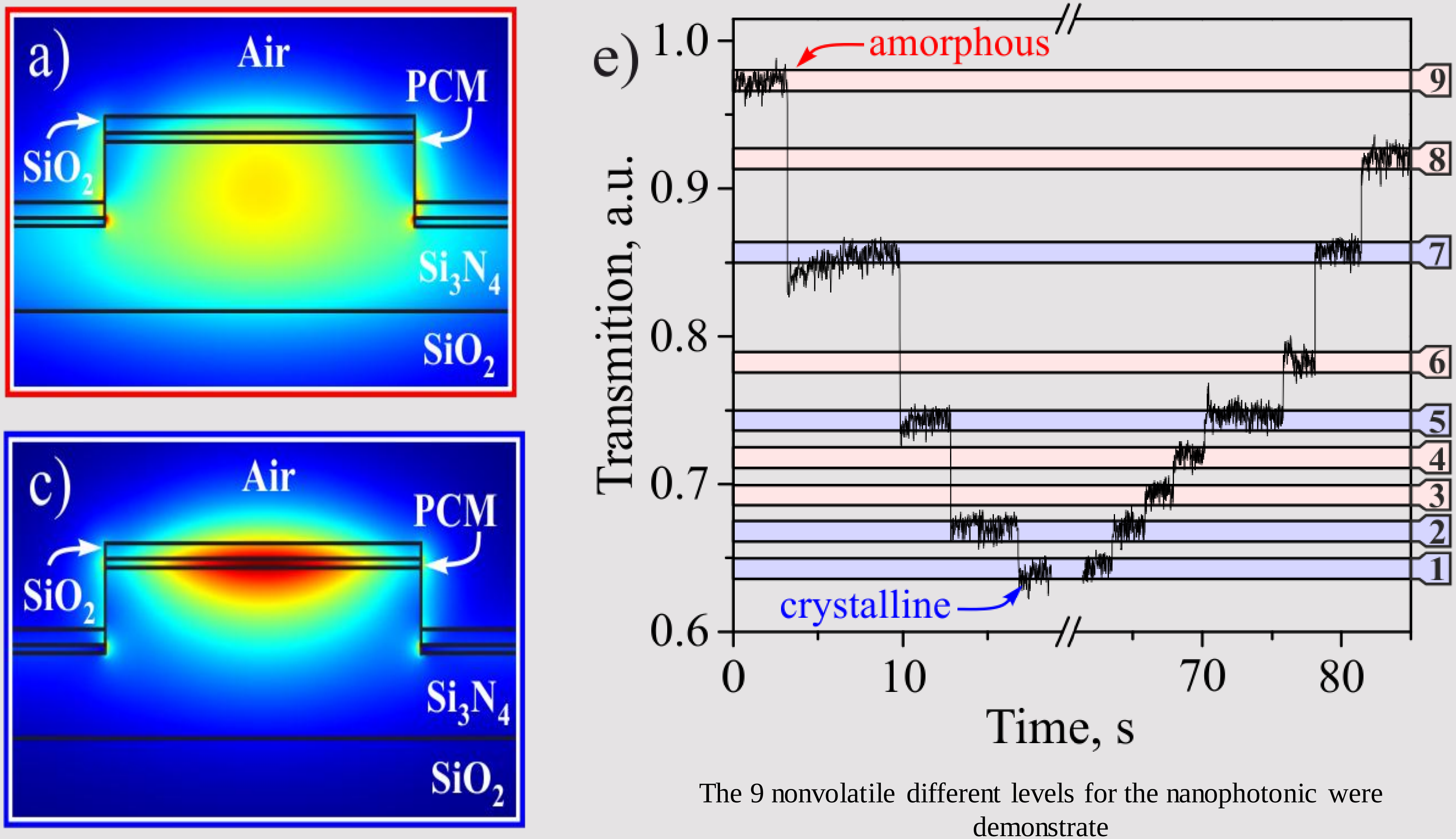

The 9 nonvolatile different levels for the nanophotonic were demonstrate

[1] S. Kozyukhin, et al. Laser-induced modification and formation of periodic surface structures (ripples) of amorphous GST225 phase change materials // Optics and Laser Technology 113 (2019) 87–94

[2] S. Kozyukhin and et al. Specific Features of Formation of Laser-Induced Periodic Surface Structures on $Ge_2Sb_2Te_5$ Amorphous Thin Films under Illumination by Femtosecond Laser Pulses // PSS:B 257 (2020) P. 1900617

Types of PCM devices

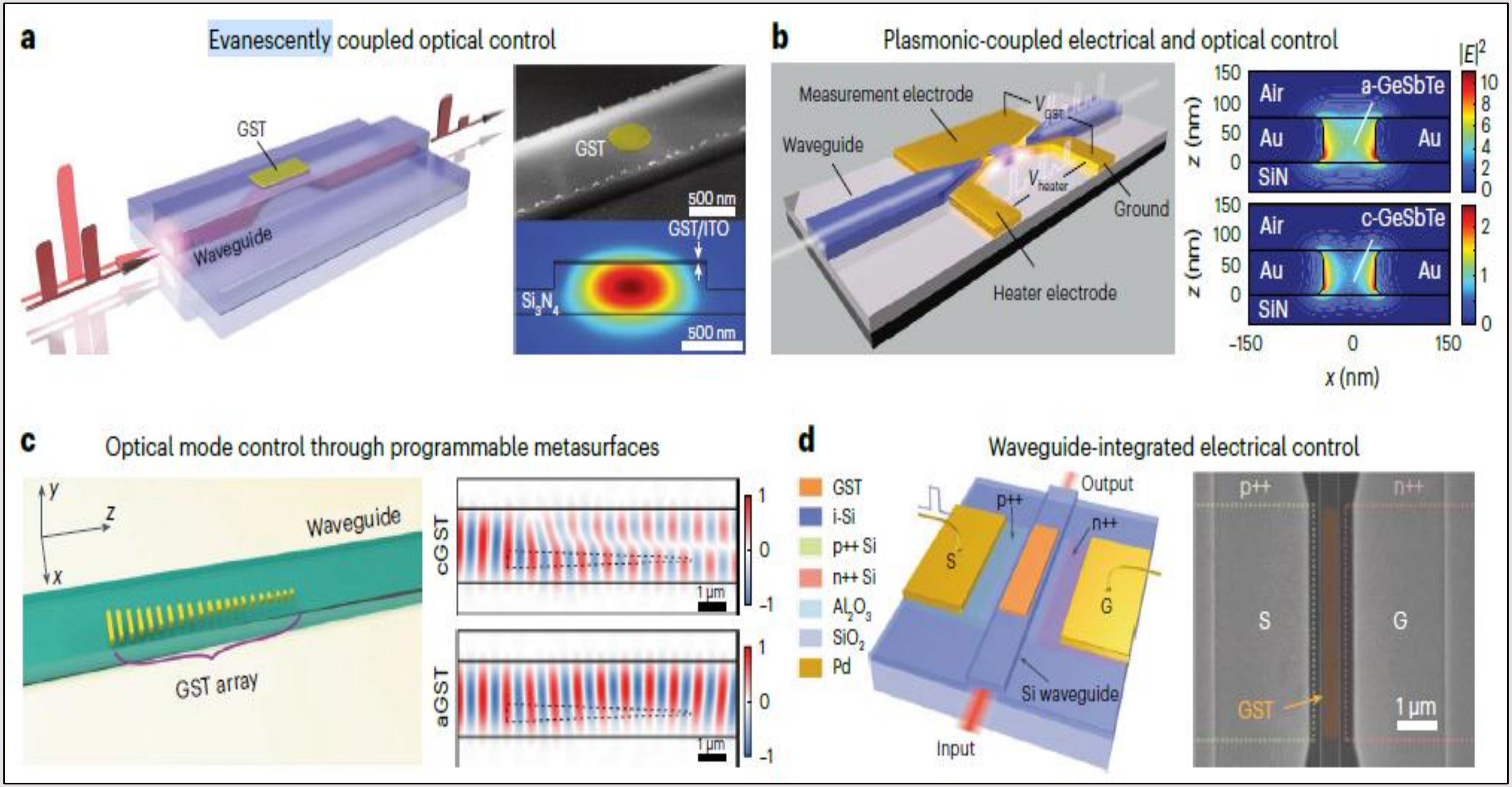

[1] N.Youngblood et al. Integrated optical memristors // Nature Photonics (2023)

PCM application

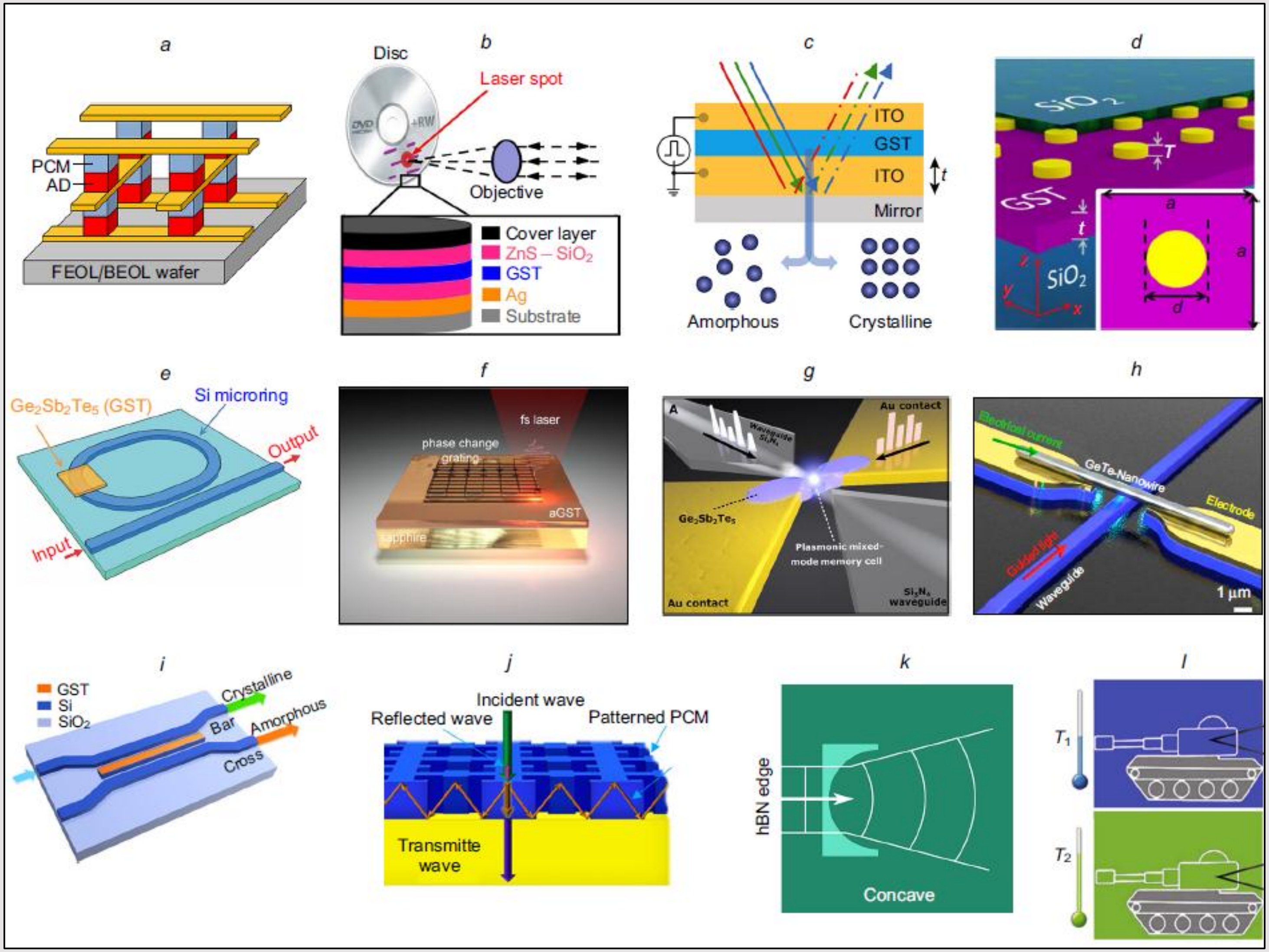

(a) 3D-Xpoint electrical memory; (b) optical discs; (c) reflective displays; (d) hybrid metasurface; (i) racetrack microresonators; (f) diffraction grattings; (g) electro-optical element based on plasmonic waveguide; (h) optoelectronic integrated cell based on thin film waveguides; (i) waveguide switcher; (j) near-IR metasurfaces; (k) lenses, prisms and other elements for the control of parameters of surface waves; (l) thermal camouflage.

Спасибо за внимание!

Lazarenko Petr
Ph.D., associate professor
National Research University of Electronic Technology (MIET)

E-mail: aka.jum@gmail.com, lpi@org.miet.ru

https://miet.ru/person/61114
ReserchID: D-9575-2014
Scopus Id=54886204100

Laboratory
Active Photonic
Materials and Devices